The Journal of Chemical Physics

RESEARCH ARTICLE | APRIL 16 2025

A general formalism to describe the stereodynamics of bond axis orientation in the scattering of a linear molecule with an atom

Max McCrea ; Matt Strutton ; Josh Featherstone ; Cornelia G. Heid ; Mark Brouard ; Pablo G. Jambrina ; F. Javier Aoiz

J. Chem. Phys. 162, 154306 (2025)
https://doi.org/10.1063/5.0261118

The Journal of Chemical Physics ARTICLE pubs.aip.org/aip/jcp

A general formalism to describe the stereodynamics of bond axis orientation in the scattering of a linear molecule with an atom

Cite as: J. Chem. Phys. 162, 154306 (2025); doi: 10.1063/5.0261118
Submitted: 29 January 2025 • Accepted: 31 March 2025 •
Published Online: 16 April 2025

Max McCrea,[1] Matt Strutton,[1] Josh Featherstone,[1] Cornelia G. Heid,[1] Mark Brouard,[1,a)] Pablo G. Jambrina,[2,b)] and F. Javier Aoiz[3,c)]

AFFILIATIONS

[1] Chemistry Research Laboratory, Department of Chemistry, University of Oxford, 12 Mansfield Road, Oxford OX1 3TA, United Kingdom
[2] Departamento de Química Física, Facultad de Ciencias Químicas, Universidad de Salamanca, 37008 Salamanca, Spain
[3] Departamento de Química Física, Facultad de Ciencias Químicas, Universidad Complutense de Madrid, 28040 Madrid, Spain

[a)] **Author to whom correspondence should be addressed:** mark.brouard@chem.ox.ac.uk
[b)] pjambrina@usal.es
[c)] aoiz@quim.ucm.es

ABSTRACT

One of the aims of the chemist is to obtain the greatest possible level of control over the outcome of a reaction. A factor that can influence such outcomes is the so-called *steric effect*. The underpinning idea of this effect is that the mutual orientation of the collision partners at the moment of collision may impact the nature of the products. The steric effect has been studied in a variety of ways, notably using optical methods, as well as making use of both magnetic and electric fields, to orient or align reactants. Here, we present a general framework for interpreting and evaluating steric effects in collisions of open shell linear molecules with an atom in the presence of an electric field. While in previous studies, the theory has been limited to the specific system of interest, such as for the end-on collisions of NO(X), this new formalism provides a fundamental basis for examining any system of this type. Some examples of the utility and power of this formalism are also provided. This theory may then be built on further in the future to provide greater insights into the stereodynamics of collisions and, hence, provide the foundation for deeper study into how the steric effect may be harnessed for control.

I. INTRODUCTION

The *steric effect* is a concept that has been embedded in chemistry since its very beginnings as a molecular science. The steric factor was introduced into chemical kinetics, somewhat phenomenologically, to account for the lower values of the rate coefficients of some reactions compared with those calculated using the simplest hard-sphere collision theory.[1,2] The underlying concept is that chemical reactions and inelastic processes are governed by specific requirements with respect to the relative orientation of the collision partners. Therefore, one of the goals of chemistry and molecular physics is to investigate how the inelastic or reactive collision probability changes when the collision partners are polarized, that is to say, how the various observables related to the (inelastic or reactive) collision dynamics are affected by certain orientations of their internuclear axes. Unveiling the relationship between the initial and final scalar and vector quantities, and in particular the polarization of the collision partners, furnishes one of the most important and intuitive concepts in chemistry: the (inelastic or reactive) collision mechanism.

A given experiment designed to study the effect of the polarization (orientation and/or alignment) on the collision dynamics consists of preparing a distribution of the internuclear axis using optical transitions or electric or magnetic fields. Ideally, one would like to make this distribution as sharp as possible in any arbitrary direction. The experiment would then require the measurement of integral (ICS) and/or differential cross sections (DCSs) for different initial internuclear axis distributions. The preparation of such axis distributions is typically made through the mediation of the rotational angular momentum. This can be achieved directly, by preparing a distribution of magnetic quantum number, m, states (which can be classically considered as the direction of the rotational angular momentum vector, $\boldsymbol{j}$), for example, via an optical transition (resonant or Raman) or by the Stark or Zeeman effect.

If the initial and final relative velocities, $\boldsymbol{k}$ and $\boldsymbol{k}'$, respectively, are known, the simplest vector correlation is $\boldsymbol{k}$–$\boldsymbol{k}'$. This correlation is described by the DCS (or angular distribution), proportional to the probability of scattering into a specific final state with a specific scattering angle, θ. DCSs are routinely measured in crossed molecular beam experiments in which the initial relative velocity of the collision partners is well-defined, and therefore, the scattering distribution after the collision event may be measured, for example, using velocity-map[3] ion imaging.[4] Of course, the $\boldsymbol{k}$ and $\boldsymbol{k}'$ vectors are not enough to fully characterize a system of interest, and even for the simplest case of a diatomic molecule colliding with an atom, four vectors are necessary to describe the system completely.[2,5] In principle, using methods to control the initial polarization of the reactants such as those presented here, as well as the detection of the product rotational angular momentum, $\boldsymbol{j}'$, one may completely describe the scattering dynamics of a system with the four-vector correlation, $\boldsymbol{k}$–$\boldsymbol{r}$–$\boldsymbol{k}'$–$\boldsymbol{j}'$, where $\boldsymbol{r}$ is the initial polarization of a specific internuclear axis. One could also measure or infer the correlation $\boldsymbol{k}$–$\boldsymbol{j}$–$\boldsymbol{k}'$–$\boldsymbol{j}'$,[6] where $\boldsymbol{j}$ is the initial polarization of the rotational angular momentum, as $\boldsymbol{j}$ and $\boldsymbol{r}$ are not independently distributed.[2] Since $\boldsymbol{j}$ describes the plane and sense of rotation of the diatom, the distribution of directions along which the internuclear axis of the diatom lies is also defined if the polarization of $\boldsymbol{j}$ is known. Most commonly, however, only three-vector correlations, such as $\boldsymbol{k}$–$\boldsymbol{k}'$–$\boldsymbol{j}'$, which specify the alignment or orientation of the final rotational angular momentum at a given scattering angle, are determined. The counterpart is the $\boldsymbol{k}$–$\boldsymbol{j}$–$\boldsymbol{k}'$ correlation, which tells us about the effect of the polarization of the initial rotational angular momentum (or the internuclear axis) on the outcome of a collision.

From a theoretical point of view, many calculations only focus on scalar properties, such as the integral cross section, the opacity functions, or the thermal rate coefficients that depend on the square of the elements of the scattering matrix, **S**. To calculate vector properties, it is necessary to consider also the phase of these elements. There are several approaches and formalisms to account for three-vector correlations. In this and previous work, we make use of the scattering angle dependent multipole coefficients or *Polarization Dependent Differential Cross Sections* (PDDCSs) that are a natural extension of the DCS with unpolarized collision partners. They quantify the dependence of the collision on the polarization of the rotational angular momentum, $\boldsymbol{j}$-PDDCSs, or of the bond axis, $\boldsymbol{r}$-PDDCSs, as a function of the scattering angle. The meaning of the latter is analogous to the $\boldsymbol{j}$-PDDCSs[7–9] except for the fact that they contain information on how the direction of the bond axis, $\boldsymbol{r}$, influences the reactivity, while the $\boldsymbol{j}$-PDDCSs are concerned with the role of the direction of the reactant's rotational angular momentum, $\boldsymbol{j}$. The PDDCSs can be readily calculated from the S-matrix at a similar computational cost to the DCS. They behave as spherical tensors (multipole moments) upon the rotation of the reference frame, and each of them is characterized by rank and component.

As in previous work, we will make the distinction between extrinsic and intrinsic polarizations.[8] The *extrinsic* polarization tells us how the collision partners have been oriented relative to each other prior to the collision and quantify the anisotropies of $\boldsymbol{j}$ or $\boldsymbol{r}$ in the asymptotic region. In contrast, the *intrinsic* polarization moments quantify the dependence of the reaction cross section on the anisotropies of the rotational angular momentum and molecular axis distributions of the reactants. They are determined by the collision dynamics rather than by external circumstances (the experimental setup). Whereas the calculations of intrinsic moments require the full S-matrix, extrinsic moments are independent of the collision dynamics. As has been shown in previous work,[8,9] the measurable DCS, subject to a given preparation of the internuclear axis, will require the combination of extrinsic and intrinsic moments.

It is important to distinguish the concepts of orientation and alignment when discussing both the initial bond vector, $\boldsymbol{r}$, and the initial rotational angular momentum, $\boldsymbol{j}$.[11,12] While both terms refer to the polarization with respect to a specific reference axis, both are required to fully describe the steric effects at play in most systems. In a diatom–atom collision, the diatom is *aligned* if $\boldsymbol{r}$ is either parallel (end-on) or perpendicular (side-on) to $\boldsymbol{k}$, as shown in Fig. 1(a). The diatom is *oriented* if the internuclear axis points in a specific direction along the axis of reference. If the direction of $\boldsymbol{r}$ is parallel or anti-parallel to the z–axis (defined by $\boldsymbol{k}$) or to the x–axis (perpendicular to $\boldsymbol{k}$), the orientation is end-on and side-on, respectively. Similarly, the system can be described in terms of both the initial and final rotational angular momenta, $\boldsymbol{j}$ and $\boldsymbol{j}'$. It is important to stress that not all molecules of interest may be both oriented and aligned in their ground state configurations: for example, molecules in $j = 1/2$, such as NO(X) in its ground state, may only be oriented with respect to a specific axis, and not aligned. From a theoretical point of view, orientation and alignment correspond to odd and even rank moments. The description of a collision with aligned molecules requires only moments whose rank is even.[7,13–20]

Here, we develop a formalism that both complements and expands upon previous work examining the stereodynamics of collisions of NO(X) with rare gases through the $\boldsymbol{r}$-PDDCSs. Indeed, we present general expressions for the $\boldsymbol{r}$-PDDCSs for atom–diatom collisions, in which the diatom is in a $^2\Pi$ state, and illustrate the significance of these moments through some experimental and theoretical examples. Note that our treatment applies to situations in which the molecules remain in well-defined j-states, and the Stark shifts induced by the applied electric field are small relative to the total energy of the experiment, the treatment of which would require full consideration of the Stark effect on the system.[21,22] New calculations are presented for the scattering of oriented NO(X, $j = 1/2$) with a range of collision partners, as well as for OH(X) + Ar, in which OH is initially oriented in the $j = 3/2$ state. For both systems,

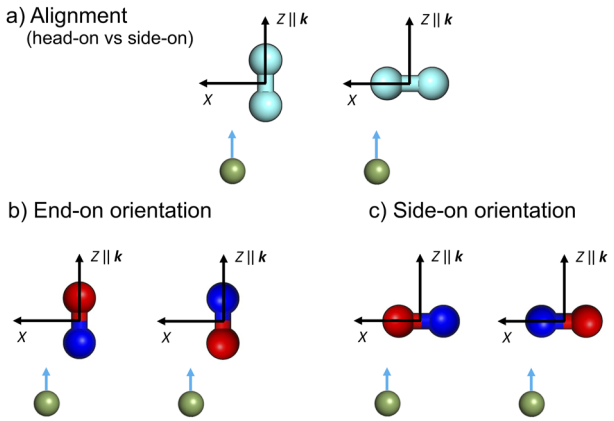

FIG. 1. Illustration of the difference between (a) alignment, (b) end-on orientation, and (c) side-on orientation of the internuclear axis ($\boldsymbol{r}$) of a diatomic molecule (*z*-axis parallel to $\boldsymbol{k}$). In panel (a), the molecule is aligned either along the *z*-axis or along the *x*-axis, with equal probabilities for either end to be pointing up or down, and left or right, leading to head-on and side-on encounters, respectively. The molecule is oriented when the internuclear axis points in a specific direction along the axis of reference. In the examples shown in panels (b) and (c), the diatomic molecule is oriented either parallel or antiparallel to the *z*−axis or the *x*−axis, respectively. Reproduced with permission from Heid *et al.*, Nat. Chem. **11**, 662–668 (2019).

comparisons are made with previous experimental results, where these are available.

II. THEORETICAL FRAMEWORK

In the following, we consider the case in which the initial quantum state of the molecule is selected by means of an electric hexapole, but the derived stereodynamic formulism is readily applicable if other methods for initial quantum state selection are employed.

A. Alignment and orientation of the internuclear axis of an open shell linear molecule by electric fields

For a pure Hund's case (a) open shell diatomic molecule, the electronic–rotational state may be written as a direct product of the rotational state $|jm\Omega\rangle$ and the electronic state $|\Lambda\Sigma\rangle$. The total angular momentum of the diatomic molecule excluding the nuclear spin is denoted by *j*, while its projection onto the internuclear axis, which is taken as the molecule body-fixed (BF) *z*-axis, and the space-fixed (SF) *Z*-axis is Ω and *m*, respectively. Λ and Σ are the projections of the electronic orbital and spin angular momentum, respectively, onto the BF axis. The rotational state wavefunction can be written in terms of Wigner rotation matrix elements,

$$|jm\Omega\rangle = \left[\frac{2j+1}{8\pi^2}\right]^{1/2} D^{j*}_{m\Omega}(\Phi_r, \Theta_r, \chi_r), \tag{1}$$

where Φ_r, Θ_r, and χ_r are the Euler angles that relate the BF and SF frames. The total wavefunction can be symmetrized as a linear combination of $+\bar{\Omega}$ and $-\bar{\Omega}$ states, where the bar represents the absolute values such that the resulting eigenfunction has a defined parity,

$$|jm\bar{\Omega}\varepsilon\bar{\Lambda}\bar{\Sigma}\rangle = \frac{1}{\sqrt{2}}\left[|jm\bar{\Omega}\rangle|\bar{\Lambda}\bar{\Sigma}\rangle + \varepsilon\,|jm-\bar{\Omega}\rangle|-\bar{\Lambda}-\bar{\Sigma}\rangle\right], \tag{2}$$

where $\varepsilon = \pm 1$. The relation between the parity *p* (symmetry with respect to inversion in the BF frame) and the symmetry index ε is $p = \varepsilon(-1)^{j-S}$, which for $S = 1/2$ can be written as $p = (-1)^{j-\varepsilon/2}$. Therefore, for each value of $\bar{\Omega}$, there are two states, known as the Λ-doublet states. States with $\varepsilon = +1$ and -1 are designated as *e* and *f* states, respectively. In what follows, we will ignore the electronic function $|\Lambda\Sigma\rangle$, as we are only interested in the sum of Λ and Σ to yield Ω.

As discussed elsewhere,[12,23] if a beam of open shell diatomic molecules with $\Lambda \geq 1$, such as NO($X^2\Pi$) or OH($X^2\Pi$), propagates along a hexapole electric field, the electric field will act as a state selector, focusing just one of the Λ-doublet states. A nonhomogeneous electric field of this kind is created by a circular arrangement of six electrodes that are alternately positively and negatively charged. This produces an electric field with magnitude,

$$E(R) = 3V_0\frac{R^2}{R_0^3}, \tag{3}$$

where *R* is the radius from the center of the hexapole, R_0 is the inner radius of the hexapole, and V_0 is the magnitude of the potential applied to each electrode. The Stark energy, assuming that the field is insufficiently strong to cause mixing of states with different values of *j*, is then given by

$$W_{\text{Stark}} = \varepsilon\left(\frac{E_\Lambda}{2} - \sqrt{\left(\frac{E_\Lambda}{2}\right)^2 + (\mu E\kappa)^2}\right), \tag{4}$$

where E_Λ is the energy splitting of the Λ-doublet states, μ is the magnitude of the electric dipole moment of the molecule, and $\kappa = m\Omega/j(j+1)$. Hence, the force experienced by the molecules in the field is described by

$$F(R) = -\frac{dW_{\text{Stark}}}{dR} = -\frac{\varepsilon F_0}{\sqrt{1+\left(\frac{E_\Lambda}{F_0 R}\right)^2}}, \tag{5}$$

where

$$F_0 = \mu\bar{\kappa}\frac{6V_0 R}{R_0^3}. \tag{6}$$

In the limit of $E_\Lambda \ll 2\,\mu\bar{\kappa}E$,

$$W_{\text{Stark}} = -\varepsilon\,\bar{\kappa}\mu\,E. \tag{7}$$

Usually, in a supersonic expansion, only the ground state is significantly populated, which for NO would be $|j = 1/2,\ m = \pm 1/2,\ \bar{\Omega} = 1/2\rangle$, and for OH $|j = 3/2,\ m = \pm 1/2, \pm 3/2,\ \bar{\Omega} = 3/2\rangle$. Before the hexapole, both Λ components are equally populated due to the small difference in energy between the *e* ($\varepsilon = +1$) and *f* ($\varepsilon = -1$) states. However, in the hexapole field, the *f* state experiences an increase in energy in the presence of an electric field and as such is low-field seeking and will be focused by the hexapole field. In contrast, the *e* component will be high-field seeking and will be defocused from the path to the interaction region. Therefore, the state that emerges from the hexapole and is focused into the interaction

region is $|jm\bar{\Omega}f\rangle$. In all cases, the m degeneracy is (partially) lifted by the Stark effect.

If, in addition, a static electric field, $\boldsymbol{E}$, is applied after the selected beam emerges from the hexapolar field, open shell molecules with permanent dipole moments can be oriented with respect to the static field of magnitude $\boldsymbol{E}$. The direction of the dipole moment of NO is from $N^{\delta-} \rightarrow O^{\delta+}$, while for OH, it is $O^{\delta-} \rightarrow H^{\delta+}$. On simple classical grounds, one would expect the dipole moment to align with the electric field. Hence, for OH, the H-end would point in the negative direction of the electric field (whose direction is taken from $+ \rightarrow -$). However, as the hexapole selects the low-field seeking f Λ-doublet level, it is the O-end of the molecule that will be oriented toward the negative electrode. Similarly, for NO, the N-end of the molecule is oriented toward the negative electrode.

As a result of the interaction with the static field, the f state evolves into a coherent linear combination of the e and f field-free states,

$$|jm_E\bar{\Omega}\boldsymbol{E}\rangle = \frac{1}{\sqrt{2}}\left(\alpha|jm_E\bar{\Omega}e\rangle + \beta|jm_E\bar{\Omega}f\rangle\right), \tag{8}$$

where m_E is the projection of the rotational angular momentum $\boldsymbol{j}$ onto the direction of the orienting static electric field. The real coefficients α and β are given by the solution of the 2×2 Stark Hamiltonian and their absolute values are given by:

$$|\alpha(E)| = \sqrt{1 - \frac{1}{\sqrt{1+E_{\text{red}}^2}}}, \quad |\beta(E)| = \sqrt{1 + \frac{1}{\sqrt{1+E_{\text{red}}^2}}}, \tag{9}$$

where the strength of the reduced electric field is

$$E_{\text{red}} = \frac{2\bar{\kappa}\mu E}{E_\Lambda}. \tag{10}$$

If $m_E > 0$, $\alpha\beta = -|\alpha\beta|$, while if $m_E < 0$, $\alpha\beta = +|\alpha\beta|$.

Taking into account Eq. (2), the oriented states, Eq. (8), can also be written as

$$|jm_E\bar{\Omega}\boldsymbol{E}\rangle = \frac{1}{2}\left[(\alpha+\beta)|jm_E\bar{\Omega}\rangle + (\alpha-\beta)|jm_E-\bar{\Omega}\rangle\right]. \tag{11}$$

The normalization of Eq. (11) implies that $\alpha^2 + \beta^2 = 2$. According to Eq. (9), $|\alpha| = |\beta| = 1$ in the high-field limit, $W_{\text{Stark}} \gg E_\Lambda \Leftrightarrow E_{\text{red}} \rightarrow \infty$. The two limiting cases correspond to pure $|j, -\tilde{m}_E, \bar{\Omega}\rangle$ and $|j, \tilde{m}_E, -\bar{\Omega}\rangle$ states for $\alpha\beta = 1$ and $\alpha\beta = -1$, respectively. In the absence of a static field, $\alpha = 0$ and $\beta = \sqrt{2}$; that is, the non-oriented f state is recovered.

Expressing the $|jm\Omega\rangle$ ket in the coordinate representation, the wavefunction can be written as

$$|jm_E\Omega\rangle = \sqrt{\frac{2j+1}{8\pi^2}}\, D^{j*}_{m_E\,\Omega}(\Phi_{\mu E}, \Theta_{\mu E}, \chi_{\mu E}), \tag{12}$$

where $\Phi_{\mu E}, \Theta_{\mu E}, \chi_{\mu E}$ are the Euler angles that define the direction of the static dipole moment (which coincides with the internuclear axis, $\boldsymbol{\mu} \uparrow\uparrow \boldsymbol{r}$) with respect to the electric field, $\boldsymbol{E}$, which is taken as the SF Z quantization axis. Using this expression, the SF extrinsic distribution of $\boldsymbol{\mu}$ can then be written as the square of the wavefunction,

$$P(\Theta_{\mu E}) = \frac{2j+1}{32\pi^2}\int_0^{2\pi}\int_0^{2\pi}\Big|(\alpha+\beta)D^j_{m_E\bar{\Omega}}(\Phi_{\mu E}, \Theta_{\mu E}, \chi_{\mu E}) + (\alpha-\beta)D^j_{m_E-\bar{\Omega}}(\Phi_{\mu E}, \Theta_{\mu E}, \chi_{\mu E})\Big|^2 \mathrm{d}\Phi_{\mu E}\,\mathrm{d}\chi_{\mu E}. \tag{13}$$

Taking into account the azimuthal symmetry of $\boldsymbol{r}$ about $\boldsymbol{E}$ and integrating over $\Phi_{\mu E}$, and $\chi_{\mu E}$, leads to

$$P(\Theta_{\mu E}) = \frac{2j+1}{8}\left\{\left[(\alpha+\beta)d^j_{m_E\bar{\Omega}}(\Theta_{\mu E})\right]^2 \tag{14}$$

$$+ \left[(\alpha-\beta)d^j_{m_E-\bar{\Omega}}(\Theta_{\mu E})\right]^2\right\}, \tag{15}$$

where $d^j_{m\Omega}(\Theta_{\mu E})$ are the reduced Wigner rotation matrix elements.

For $j = 1/2$, $\bar{\Omega} = 1/2$, and $\tilde{m}_E = 1/2$, the above expression turns out to be

$$P(\Theta_{\mu E}) = \frac{1}{4}\left[(\alpha+\beta)^2\cos^2(\Theta_{\mu E}/2) + (\alpha-\beta)^2\sin^2(\Theta_{\mu E}/2)\right] = \frac{1}{2}(1 - |\alpha\beta|\cos\Theta_{\mu E}). \tag{16}$$

In the field, f Λ-doublet states correspond to $|jm_E\Omega\rangle$ states with $\Omega m_E < 0$ (opposite signs). Equation (16) can be recast in terms of Legendre polynomials, $P_k(\cos\Theta_{\mu E})$,

$$P(\Theta_{\mu E}) = \frac{1}{2}[1 - |\alpha\beta|\, P_1(\cos\Theta_{\mu E})]. \tag{17}$$

For $j = 3/2$, $\bar{\Omega} = 3/2$, and $\tilde{m}_E = 3/2$,

$$P(\Theta_{\mu E}) = \frac{1}{2}\left[(\alpha+\beta)^2\cos^6(\Theta_{\mu E}/2) + (\alpha-\beta)^2\sin^6(\Theta_{\mu E}/2)\right] = \frac{1}{2}\left[1 - \frac{9}{5}\,|\alpha\,\beta|\, P_1(\Theta_{\mu E}) + P_2(\Theta_{\mu E}) - \frac{1}{5}\,|\alpha\,\beta| P_3(\cos\Theta_{\mu E})\right]. \tag{18}$$

Equations (17) and (18) are particular cases of the general expression for the preparation of internuclear axes,

$$P(\Theta_{\mu E}) = \sum_{k=0}^{2j}\left(\frac{2k+1}{2}\right)\mathscr{A}_0^{(k)}\, P_k(\cos\Theta_{\mu E}), \tag{19}$$

for which the respective $\mathscr{A}_0^{(k)} = \langle P_k(\cos\Theta_{\mu E})\rangle$ coefficients are $\mathscr{A}_0^{(0)} = 1$ and $\mathscr{A}_0^{(1)} = -\frac{1}{3}|\alpha\beta|$ for $j = 1/2$ and $m_E = 1/2$. For $j = 3/2$, $\bar{\Omega} = 3/2$, and $m_E = 3/2$, the extrinsic polarization parameters are $\mathscr{A}_0^{(0)} = 1$, $\mathscr{A}_0^{(1)} = -\frac{3}{5}|\alpha\beta|$, $\mathscr{A}_0^{(2)} = \frac{1}{5}$, and $\mathscr{A}_0^{(3)} = -\frac{1}{35}|\alpha\beta|$, and for $j = 3/2$, $\bar{\Omega} = 3/2$, and $m_E = 1/2$, the extrinsic polarization parameters are $\mathscr{A}_0^{(0)} = 1$, $\mathscr{A}_0^{(1)} = -\frac{1}{5}|\alpha\beta|$, $\mathscr{A}_0^{(2)} = -\frac{1}{5}$, and $\mathscr{A}_0^{(3)} = \frac{3}{35}|\alpha\beta|$. Note that the even (alignment) moments are independent of the $\alpha\beta$ factor.

Equation (19) can be derived in the context of the axis distribution for a symmetric top when an ensemble of molecules is in a single state $|jm_E\Omega\rangle$, as in the present case.[24] It can be easily shown that the coefficients are then given by

$$\mathscr{A}_0^{(k)} = \begin{cases} -|\alpha\beta|\langle j\tilde{m}_E, k0|j\tilde{m}_E\rangle.\langle j\bar{\Omega}, k0|j\bar{\Omega}\rangle, & k \text{ odd}, \\ \langle j\tilde{m}_E, k0|j\tilde{m}_E\rangle.\langle j\bar{\Omega}, k0|j\bar{\Omega}\rangle, & k \text{ even}, \end{cases} \tag{20}$$

where $\langle \cdots, \cdots | \cdots \rangle$ are the Clebsch–Gordan coefficients and k is the rank of the polarization moment.

To illustrate the degree of orientation that can be achieved using hexapole selection and electric field orientation, the experimental internuclear axis distributions for $NO(X^2\Pi_{1/2})$[23,25] and $OH(X^2\Pi_{3/2})$[26,27] are shown in Fig. 2. In particular, the distribution of internuclear axes obtained for the $NO(X^2\Pi_{1/2})$ hexapole selection of the single $|j = 1/2, m, \bar{\Omega} = 1/2, f\rangle$ state and subsequent orientation with an electric field is shown in the top panel of Fig. 2. The left panel shows the r-portrait,[8,28] whereas the right panel shows the corresponding stereographic projection. The orientation achieved under our experimental conditions[23,25,29] is indicated in the figure with pink shading, while that obtained in the high-field limit is represented with blue shading. The values of $|\alpha|$ and $|\beta|$ are also given. The isotropic gray shading represents the axis distribution of the pure $|j = 1/2, \bar{\Omega} = 1/2, f\rangle$ state. Since, for $j = 1/2$, no alignment can be obtained, in the isotropic field-free case, the resulting distribution corresponds to $\mathcal{A}_0^{(1)} = 0$ ($|\alpha\beta| = 0$) in Eq. (17).

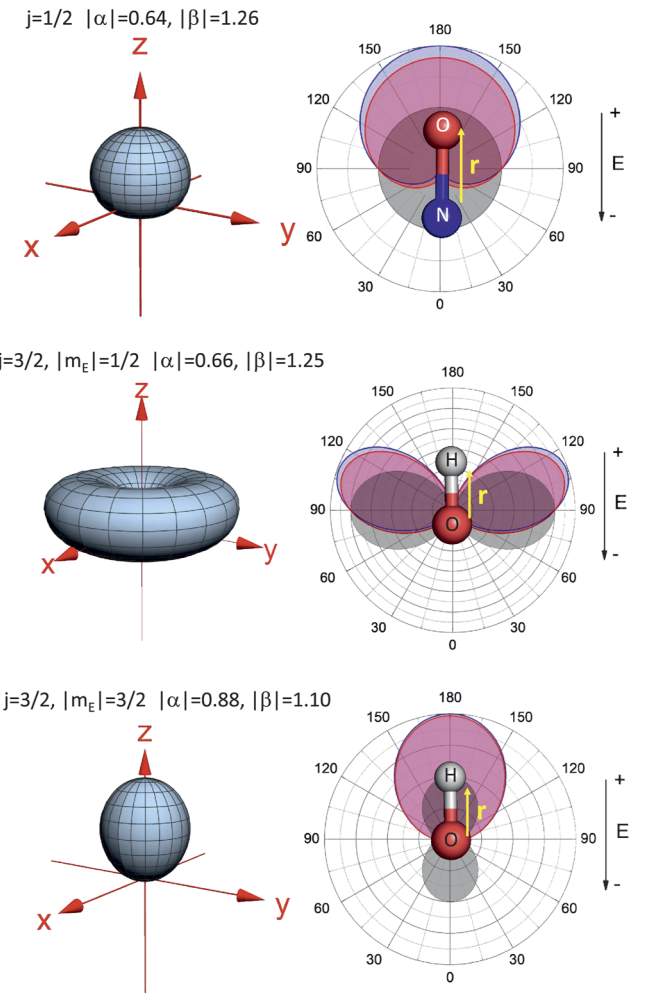

FIG. 2. Left panels: ***r***-portraits of the axis distributions of NO(X) (upper row) and OH(X) (middle and bottom rows) in an electric field. The extent of polarization is calculated with the values of $|\alpha|$ and $|\beta|$ shown in the figures using Eq. (19) with the respective values of the extrinsic ***r***-polarization parameters given by Eq. (20). The right panels show the corresponding stereographic projections of the angular axis distributions of NO(X) and OH(X) at the field strengths used in the experiments described in the text (pink shading), or at an infinite field (blue shading). The hypothetical field-free bond axis distributions with the selected values of $\tilde{m}_E$ are indicated by the gray shaded area.

Similar plots are shown in the bottom two panels of Fig. 2 for the hexapole selection of $OH(X^2\Pi)$, followed by its orientation with a static electric field.[26] By virtue of the Stark effect, the m degeneracy is broken for the $\tilde{m}_E = 1/2$ and $\tilde{m}_E = 3/2$ states. The middle panel represents the orientation experimentally achieved with $|j = 3/2, \tilde{m}_E = 1/2, \bar{\Omega} = 3/2, \boldsymbol{E}\rangle$, whereas the bottom one is for the prepared $|j = 3/2, \tilde{m}_E = 3/2, \bar{\Omega} = 3/2, \boldsymbol{E}\rangle$ state. It is worth noting that the hypothetical field-free $|j = 3/2, \tilde{m}_E = 1/2, \bar{\Omega} = 3/2, e\rangle$ and $|j = 3/2, \tilde{m}_E = 3/2, \bar{\Omega} = 3/2, e\rangle$ states are aligned, as indicated in Fig. 2.

B. Differential scattering of oriented molecules

Here, we will present the theory concerning the effect of an arbitrary orientation of internuclear axis on the differential cross section.

The expression for state-to-state DCSs when both initial and final states are completely defined is

$$d\sigma(jm\,\bar{\Omega}\varepsilon \to j'm'\,\bar{\Omega}'\varepsilon') = \left|f_{j'm'\bar{\Omega}'\varepsilon',\,jm\bar{\Omega}\varepsilon}(\theta)\right|^2, \tag{21}$$

where $f_{j'm'\bar{\Omega}'\varepsilon',jm\bar{\Omega}\varepsilon}(\theta)$ is the scattering amplitude whose explicit expression may be found elsewhere.[13,30] When the orbital angular momentum representation is used in the scattering expressions, m and m' refer to the projections of $\boldsymbol{j}$ and $\boldsymbol{j}'$ along the initial relative velocity, $\boldsymbol{k}$. The vibrational quantum number will be disregarded as we focus on rotational energy transfer.

To simplify the notation, hereinafter, we shall write for given j, j', $\bar{\Omega}$, and $\bar{\Omega}'$ values,

$$f_{j'm'\bar{\Omega}'\varepsilon',\,jm\bar{\Omega}\varepsilon}(\theta) \equiv F_{m'\varepsilon',\,m\varepsilon}. \tag{22}$$

An important property is the symmetry rule affecting the scattering amplitudes,[13,30]

$$F_{-m'\varepsilon',-m\varepsilon} = \varepsilon\varepsilon'(-1)^{m-m'}F_{m'\varepsilon',\,m\varepsilon}. \tag{23}$$

Now, we consider two reference frames, as illustrated in Fig. 3. The laboratory (LAB) frame has been described in Sec. II A: the direction of the static orienting field, $\boldsymbol{E}$, is the Z-axis. The equations related to the preparation of internuclear axes (extrinsic distributions) are referenced to this frame. For a diatomic molecule, it suffices to specify an angle between the internuclear axis, $\boldsymbol{r}$ ($\|\boldsymbol{\mu}$), and $\boldsymbol{E}$, $\Theta_{\mu E}$. The projection of the molecular rotational angular momentum, $\boldsymbol{j}$, in this frame is m_E. We now define the orientation of the electric field in the second frame, the scattering frame, as shown in the right panel of Fig. 3, defined by the initial relative velocity, $\boldsymbol{k}$, along the z-axis, and $\boldsymbol{kk}'$ (xz plane) as the origin of the azimuthal angle. The projection of $\boldsymbol{j}$ onto $\boldsymbol{k}$ is m. The direction of $\boldsymbol{E}$ in this frame is given by the polar and azimuthal angles θ_E and ϕ_E, respectively.

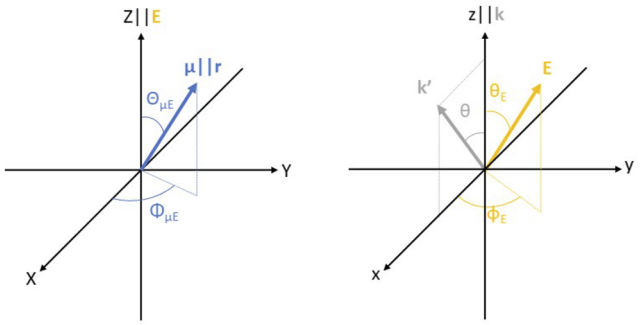

FIG. 3. Left panel: sketch of the laboratory (LAB) frame in which the orienting electric field, $\boldsymbol{E}$, is along the Z-axis. The direction of the electric dipole moment (and of the molecular axis) is defined by the $\Theta_{\mu E}$ and $\Phi_{\mu E}$ angles. Right panel: scattering frame with the initial relative velocity, $\boldsymbol{k}$, along the z-axis and the xz-hemiplane defined by $\boldsymbol{k}$ and recoil relative velocity, $\boldsymbol{k}'$. In this frame, the orienting field is defined by the angles θ_E and ϕ_E. In the particular case of the $+z$ and $-z$ orientations, the electric field is parallel ($\Theta_{\mu E} = 0°$) and antiparallel ($\Theta_{\mu E} = 180°$) to $\boldsymbol{k}$, respectively. If $\boldsymbol{E}$ is along the $+x$ ($-x$) axis, the direction of $\boldsymbol{E}$ is given by $\theta_E = 90°$ and $\phi_E = 0°$ ($\theta_E = 90°$ and $\phi_E = 180°$).

The expression for a rotational state with its projection along $\boldsymbol{E}$, Eq. (11), in terms of those states whose quantization axis is taken along $\boldsymbol{k}$ can be written as

$$|jm_E\bar{\Omega}\varepsilon\rangle = \sum_m D^j_{m\ m_E}(\phi_E,\theta_E,0)|jm\bar{\Omega}\varepsilon\rangle, \tag{24}$$

where $D^j_{m\ m_E}(\phi_E,\theta_E,0)$ ($\equiv D^j_{m\ m_E}$ hereinafter) is a rotation matrix element with angles θ_E and ϕ_E that relate the LAB frame to the scattering frame. It should be stressed that the projection of $\boldsymbol{j}$ onto the orienting field, m_E, may be positive or negative. Accordingly, the scattering amplitude when the initial states are referenced to the LAB frame can be written as

$$F_{m'\varepsilon'\ m_E\varepsilon} = \sum_m D^j_{m\ m_E}\, F_{m'\varepsilon'\ m\varepsilon}. \tag{25}$$

Considering Eq. (8), the state vector in the presence of the field (the coherent superposition of the e and f states) can be expressed as

$$|jm_E\bar{\Omega}\ \hat{E}\rangle = \frac{1}{\sqrt{2}}\sum_m D^j_{m\ m_E}\left[\alpha|jm\bar{\Omega}e\rangle + \beta|jm\bar{\Omega}f\rangle\right]. \tag{26}$$

The scattering amplitude from the state $|jm_E\bar{\Omega}\ \boldsymbol{E}\rangle$ to a given final state $|j'm'\bar{\Omega}'\varepsilon'\rangle$ can be written as

$$F_{m'\varepsilon'\ m_E\hat{E}} = \frac{1}{\sqrt{2}}\sum_m D^j_{m\ m_E}\left[\alpha F_{m'\varepsilon'\ me} + \beta F_{m'\varepsilon'\ mf}\right]. \tag{27}$$

The simplest case arises when the static orienting field is parallel ($\theta_E = 0°$) or antiparallel ($\theta_E = 180°$) to $\boldsymbol{k}$, when $m_E = \pm m$.

The next step consists of constructing the DCS for the $|jm_E\bar{\Omega}\ \boldsymbol{E}\rangle \rightarrow |j'm'\bar{\Omega}'\varepsilon'\rangle$ transition. Because the Λ-doublet splittings in NO(X) and OH(X) increase significantly with j, it is possible to control the conditions of the experiment such that only the initial Λ-doublet states are mixed in the field, and hence, we can write

$$\mathrm{d}\sigma(jm_E\ \bar{\Omega}\hat{E} \rightarrow j'm'\ \bar{\Omega}'\varepsilon') = \left|F_{m'\varepsilon'\ m_E\hat{E}}\right|^2. \tag{28}$$

Summing over all final m' states,

$$\begin{aligned}\mathrm{d}\sigma(jm_E\ \bar{\Omega}\hat{E} \rightarrow j'\ \bar{\Omega}'\varepsilon') &= \sum_{m'}\left|F_{m'\varepsilon'\ m_E\hat{E}}\right|^2 \\ &= \frac{1}{2}\sum_{m'}\left|\sum_m D^j_{m\ m_E}\left(\alpha F_{m'\varepsilon'\ me} + \beta F_{m'\varepsilon'\ mf}\right)\right|^2.\end{aligned} \tag{29}$$

Introducing a short-hand notation, the product of scattering amplitudes can be written as

$$Q_{m_1\varepsilon_1 m_2\varepsilon_2} \equiv \sum_{m'} F_{m'\varepsilon' m_1\varepsilon_1} F^*_{m'\varepsilon' m_2\varepsilon_2}. \tag{30}$$

A summary of the detailed properties of these products of scattering amplitudes is presented in Appendix A. Employing this notation, Eq. (29) can then be expanded,

$$\begin{aligned}\mathrm{d}\sigma(jm_E\ \bar{\Omega}\hat{E} \rightarrow j'\ \bar{\Omega}'\varepsilon') = \frac{1}{2}\Bigg[&\alpha^2\sum_{m_1,m_2} D^j_{m_1\ m_E} D^{j*}_{m_2\ m_E} Q_{m_1 e, m_2 e} \\ &+ \alpha\beta\sum_{m_1,m_2} D^j_{m_1\ m_E} D^{j*}_{m_2\ m_E}\left(Q_{m_1 f, m_2 e}\right. \\ &\left.+\ Q_{m_1 e, m_2 f}\right) \\ &+ \beta^2\sum_{m_1,m_2} D^j_{m_1\ m_E} D^{j*}_{m_2\ m_E} Q_{m_1 f, m_2 f}\Bigg].\end{aligned} \tag{31}$$

Note that in Eq. (31), m_E can have positive, $+\bar{m}_E$, or negative, $-\bar{m}_E$, values. As indicated in Sec. II A, when $m_E > 0$, $\alpha\beta = -|\alpha\beta|$, and when $m_E < 0$, $\alpha\beta = +|\alpha\beta|$.

To obtain the final expression for the DCS, it suffices to average over the two values (positive and negative) of m_E,

$$\begin{aligned}\mathrm{d}\sigma(j\bar{m}_E\ \bar{\Omega}\hat{E} \rightarrow j'\ \bar{\Omega}'\varepsilon') = \frac{1}{2}\Big[&\mathrm{d}\sigma(jm_E\ \bar{\Omega}\hat{E} \rightarrow j'\ \bar{\Omega}'\varepsilon') \\ &+ \mathrm{d}\sigma(j\ -m_E\ \bar{\Omega}\hat{E} \rightarrow j'\ \bar{\Omega}'\varepsilon')\Big].\end{aligned} \tag{32}$$

Equations (31) and (32) can be directly used to obtain the DCS for any value of j, $\bar{\Omega}$, and $\bar{m}_E$ once the scattering amplitudes have been calculated. However, after some algebra and making use of the relation between the products of scattering amplitudes in Appendix A, it is possible to derive simplified expressions with explicit dependence on the angles θ_E and ϕ_E, which define the orientation of the electric field in the $\boldsymbol{kk}'$ frame, as explained in Appendix B. For any value of j, Eq. (32) can be written as

$$\begin{aligned}&\left[\mathrm{d}\sigma(j\bar{m}_E\bar{\Omega}\ \hat{E} \rightarrow j'\ \bar{\Omega}'\varepsilon')\right]_{\theta_E}^{\phi_E} \\ &\quad= \sum_k (2k+1)\mathscr{A}_0^{(k)}\sum_{q=-k}^{k} C_{kq}(\theta_E,\phi_E)\tilde{R}_q^{(k)}(\theta),\end{aligned} \tag{33}$$

where $C_{kq}(\theta_E, \phi_E)$ are the modified spherical harmonics, and $\tilde{R}_q^{(k)}(\theta)$ are the unnormalized $\boldsymbol{r}$-PDDCSs defined by

$$\tilde{R}_q^{(\text{even } k)}(\theta) = \frac{1}{2(2j+1)} \frac{1}{\langle j\bar{\Omega}, k0 | j\bar{\Omega}\rangle} \sum_m \langle jm, kq | j(m+q)\rangle \times \sum_{\varepsilon=e,f} \gamma_\varepsilon^2 \; Q_{m\varepsilon(m+q)\varepsilon} \tag{34}$$

and

$$\tilde{R}_q^{(\text{odd } k)}(\theta) = \frac{1}{2(2j+1)} \frac{1}{\langle j\bar{\Omega}, k0 | j\bar{\Omega}\rangle} \sum_m \langle jm, kq | j(m+q)\rangle \times \sum_{\substack{\varepsilon_1 = e,f \\ \varepsilon_1 \neq \varepsilon_2}} Q_{m\varepsilon_1(m+q)\varepsilon_2}, \tag{35}$$

where $\gamma_\varepsilon = \alpha$ or β when $\varepsilon = e$ or f, respectively. The derivations of the expressions for these moments are given in Appendix B.

In Eq. (33), all extrinsic polarization effects (those imparted by the preparation of the system) are encapsulated in the $\mathscr{A}_0^{(k)}$ moments, while intrinsic polarization effects (those that depend on the collision dynamics regardless of the specific preparation of the reactants) are included in $\tilde{R}_q^{(k)}(\theta)$.

Note that the $\tilde{R}_0^{(0)}(\theta)$ moment for a given j state can be written as

$$\tilde{R}_0^{(0)}(\theta) = \frac{\alpha^2}{2} \; \mathrm{d}\sigma(j, \bar{\Omega}, e \to j', \bar{\Omega}', \varepsilon') + \frac{\beta^2}{2} \; \mathrm{d}\sigma(j, \bar{\Omega}, f \to j', \bar{\Omega}', \varepsilon'). \tag{36}$$

Therefore, the isotropic DCS in the presence of the orienting field is the average of the $e \to \varepsilon'$ and $f \to \varepsilon'$ DCSs weighted by the α^2 and β^2 coefficients. This is in contrast to the DCS in the absence of the field for the f selected state that is given by Eq. (36) with $\alpha = 0$ and $\beta = \sqrt{2}$. We can also define the normalized $\boldsymbol{r}$-PDDCSs, $R_q^{(k)}(\theta)$, such that

$$\tilde{R}_q^{(k)}(\theta) = \frac{\sigma_{\text{iso}}}{2\pi} R_q^{(k)}(\theta), \tag{37}$$

where σ_{iso}, for given j, Ω, j', and Ω', can be written as

$$\sigma_{\text{iso}} = 2\pi \int_{-1}^{1} \tilde{R}_0^{(0)} \mathrm{d}\cos\theta = \frac{\alpha^2}{2} \sigma_{e\to\varepsilon'} + \frac{\beta^2}{2} \sigma_{f\to\varepsilon'} \tag{38}$$

and is the isotropic integral cross section in the field. Note that, as with the isotropic DCS in the field, the isotropic ICS in the presence of the orienting field is the average of the $e \to \varepsilon'$ and $f \to \varepsilon'$ ICSs weighted by the α^2 and β^2 coefficients.

By making use of the fact that for achiral systems, the $\boldsymbol{r}$-PDDCSs are real, which implies that $R_q^{(k)}(\theta) = (-1)^q R_{-q}^{(k)}(\theta)$, we can rewrite Eq. (33) to obtain

$$\left[\mathrm{d}\sigma(j\tilde{m}_E \; \bar{\Omega} \; \hat{E} \to j' \; \bar{\Omega}'\varepsilon')\right]_{\theta_E}^{\phi_E} = \frac{\sigma_{\text{iso}}}{2\pi} \sum_k^{2j} (2k+1) \mathscr{A}_0^{(k)} \sum_{q=0}^{k} \frac{2}{1+\delta_{q0}} R_q^{(k)}(\theta) C_{kq}(\theta_E, 0) \cos(q\phi_E). \tag{39}$$

A particular case is when $\theta_E = 90°$ and $\phi_E = 90°$ or 270°, that is, when the field is oriented along the y-axis (perpendicular to the scattering plane). In this case, all orientation terms in Eq. (39), with k odd, vanish and only the alignment terms, including $k = 0$, remain.

The intrinsic $\boldsymbol{r}$-polarization parameters, which quantify the effect of orientation on the integral cross section, are defined as

$$r_q^{(k)} = \int_{-1}^{1} R_q^{(k)}(\theta) \mathrm{d}\cos\theta. \tag{40}$$

Integrating Eq. (33) over the scattering angle for a given orientation of the orienting field with respect to the scattering frame yields an integral cross section that can be expressed as

$$[\sigma]_{\theta_E}^{\phi_E} = \frac{\sigma_{\text{iso}}}{2\pi} \sum_{k,q} (2k+1) r_q^{(k)} \mathscr{A}_0^{(k)} \; C_{kq}(\theta_E, \phi_E). \tag{41}$$

Further integration over the azimuthal angle between the scattering plane and the plane defined by $\boldsymbol{k}$ and $\boldsymbol{E}$ leads to

$$[\sigma]_{\theta_E} = \sigma_{\text{iso}} \sum_k (2k+1) r_0^{(k)} \mathscr{A}_0^{(k)} \; C_{k0}(\theta_E, 0). \tag{42}$$

In the particular case of $\boldsymbol{E}$ oriented along the relative velocity vector, where $\theta_E = 0$ or π ($\pm z$ orientation), there is azimuthal symmetry, and integration over ϕ_E is equivalent to multiplying by 2π,

$$\begin{aligned} [\sigma]_{\theta_E=0} &= \sigma_{\text{iso}} \sum_k (2k+1) r_0^{(k)} \mathscr{A}_0^{(k)}, \\ [\sigma]_{\theta_E=180°} &= \sigma_{\text{iso}} \sum_k (2k+1)(-1)^k r_0^{(k)} \mathscr{A}_0^{(k)}. \end{aligned} \tag{43}$$

Finally, the relationship between the $\boldsymbol{r}$-PDDCSs and $\boldsymbol{j}$-PDDCSs,[8] $U_q^{(k)}(\theta)$, for a superposition of Λ-doublet states, is discussed in detail in Appendix C. It is shown there that

$$\tilde{R}_q^{(k)}(\theta) = \frac{U_q^{(k)}(\theta)}{\langle j\bar{\Omega}\; k0 | j\bar{\Omega}\rangle}. \tag{44}$$

C. Differential scattering for $j = 1/2$

As an example, for $j = 1/2$ such as in NO(X) in its ground rovibrational state, using Eq. (39) and the expressions of the $\boldsymbol{r}$-PDDCSs, Eqs. (34) and (35), for $j = 1/2$, can be written as

$$\begin{aligned} &\left[\mathrm{d}\sigma(j\tilde{m}_E \; \bar{\Omega} \; \hat{E} \to j' \; \bar{\Omega}'\varepsilon')\right]_{\theta_E}^{\phi_E} \\ &= \frac{\sigma_{\text{iso}}}{2\pi} \left\{ R_0^{(0)}(\theta) + 3\mathscr{A}_0^{(1)} \left[R_0^{(1)}(\theta) P_1(\cos\theta_E) + 2R_1^{(1)}(\theta) C_{11}(\theta_E, 0) \cos\phi_E \right] \right\}, \end{aligned} \tag{45}$$

where the orientation moment in the laboratory frame is $\mathscr{A}_0^{(1)} = -\frac{1}{3}|\alpha\beta|$, and σ_{iso} is given by Eq. (38).

Evaluating the expressions of the $\boldsymbol{r}$-PDDCS for this particular case leads to

$$\left[\mathrm{d}\sigma(j\bar{m}_E\bar{\Omega}\,\hat{E}\to j'\,\bar{\Omega}'\varepsilon')\right]_{\theta_E}^{\phi_E} = \frac{1}{2}\left[\alpha^2 Q_1 - |\alpha\beta|\cos\theta_E\,Q_2 - |\alpha\beta|\sin\theta_E\,\cos\phi_E\,Q_3 + \beta^2\,Q_4\right], \tag{46}$$

where

$$Q_1 = Q_{1/2e,1/2e} = \sum_{m'} |F_{m'\varepsilon'\ 1/2e}|^2, \tag{47}$$

$$Q_2 = Q_{1/2e,1/2f} + Q_{1/2f,1/2e}, \tag{48}$$

$$Q_3 = Q_{1/2e,-1/2f} + Q_{1/2f,-1/2e}, \tag{49}$$

$$Q_4 = Q_{1/2f,1/2f} = \sum_{m'} |F_{m'\varepsilon'\ 1/2f}|^2. \tag{50}$$

Comparing Eqs. (45) and (46), and bearing in mind that $C_{11}(\theta,0) = -1/\sqrt{2}\sin\theta$,

$$\tilde{R}_0^{(0)}(\theta) = \frac{1}{2}(\alpha^2 Q_1 + \beta^2 Q_4), \tag{50}$$

$$\tilde{R}_0^{(1)}(\theta) = \frac{1}{2}Q_2, \tag{51}$$

$$\tilde{R}_1^{(1)}(\theta) = -\frac{1}{2\sqrt{2}}Q_3, \tag{52}$$

which agrees with our previous work.[10] In the case of $j = 1/2$, in which there are no alignment terms with $k > 0$, the differential cross section when the orienting field is along y is simply $\tilde{R}_0^{(0)}$.

The integral steric asymmetry (ISA) measures the preference of the scattering event for one orientation over its opposite. In particular, for end-on ($\pm z$, $\theta_E = 0°$ or 180°) and side-on ($\pm x$, $\theta_E = 90°$, $\phi_E = 0°$ or 180°) orientations, the respective definitions are

$$S_z = \frac{\sigma_{-z} - \sigma_{+z}}{\sigma_{-z} + \sigma_{+z}} = \frac{\sigma_{\theta_E=180°} - \sigma_{\theta_E=0°}}{\sigma_{\theta_E=180°} + \sigma_{\theta_E=0°}}, \tag{53}$$

$$S_x = \frac{\sigma_{+x} - \sigma_{-x}}{\sigma_{+x} + \sigma_{-x}} = \frac{\sigma_{\theta_E=90°}^{\phi_E=0°} - \sigma_{\theta_E=90°}^{\phi_E=180°}}{\sigma_{\theta_E=90°}^{\phi_E=0°} + \sigma_{\theta_E=90°}^{\phi_E=180°}}. \tag{54}$$

The differential steric asymmetry (DSA) resolves this preference over the scattering angle, θ. It is given analogously for both orientations,

$$\mathrm{d}\sigma_{\mathrm{diff}}^z(\theta) = \frac{\mathrm{d}\sigma_{-z}(\theta) - \mathrm{d}\sigma_{+z}(\theta)}{\mathrm{d}\sigma_{-z}(\theta) + \mathrm{d}\sigma_{+z}(\theta)}, \tag{55}$$

$$\mathrm{d}\sigma_{\mathrm{diff}}^x(\theta) = \frac{\mathrm{d}\sigma_{+x}(\theta) - \mathrm{d}\sigma_{-x}(\theta)}{\mathrm{d}\sigma_{+x}(\theta) + \mathrm{d}\sigma_{-x}(\theta)}. \tag{56}$$

In the specific case of NO(X, $j = 1/2$) in an electric field, the ISAs become

$$S_z = |\alpha\beta|\frac{r_0^{(1)}}{r_0^{(0)}} = |\alpha\beta| r_0^{(1)}, \tag{57}$$

$$S_x = |\alpha\beta|\frac{\sqrt{2}r_1^{(1)}}{r_0^{(0)}} = |\alpha\beta|\sqrt{2}r_1^{(1)} \tag{58}$$

as $r_0^{(0)} \equiv 1$. Analogously, the DSAs become

$$\mathrm{d}\sigma_{\mathrm{diff}}^z(\theta) = |\alpha\beta|\frac{R_0^{(1)}(\theta)}{R_0^{(0)}(\theta)}, \tag{59}$$

$$\mathrm{d}\sigma_{\mathrm{diff}}^x(\theta) = |\alpha\beta|\frac{\sqrt{2}R_1^{(1)}(\theta)}{R_0^{(0)}(\theta)}. \tag{60}$$

Note that an important advantage of using the present formalism is that the expressions for any arbitrary direction of the orienting field can be readily derived from the above equations.

III. APPLICATIONS

A. Computation procedures

In the following examples, the quantum mechanical (QM) calculations were performed using the HIBRIDON 4 suite of codes.[31–33] NO(X) + Ar calculations used the V_{sum} and V_{diff} Potential Energy Surfaces (PESs) of Alexander,[34] which treat NO as a rigid rotor. Calculations were performed at collision energies of 530 and 651 cm^{-1} to match those employed in the experiments for spin–orbit conserving and changing collisions, respectively.[29] Further details of these calculations are as described in Ref. 29. The approximate QM data for NO + N_2 were obtained treating N_2 as a pseudo-atom using PESs of Wen *et al.*, averaged over N_2 orientations.[35] The collision energy for these calculations was 845 cm^{-1}. The OH(X) + Ar QM data used the PESs of Klos *et al.* and a collision energy of 746 cm^{-1}.[36] These calculations employed $J_{\max} = 200.5$ and $R_{\max} = 150$ bohrs.

Quasi-classical trajectory (QCT) calculations were also performed, in which the collision partners were treated as classical particles propagating on the appropriate V_{sum} PES. The same V_{sum} PES was used as in the QM calculations, and the calculations were performed at the same collision energies noted above.[29]

B. ISAs for NO($X^2\Pi$) collision systems

The simplest use of this framework is through the integral steric asymmetry (ISA) for collisions involving NO($X^2\Pi$, $j = 1/2$, $\bar{\Omega} = 1/2$). In Fig. 4, experimental ISAs for the scattering of NO($X^2\Pi$, $j = 1/2$, $\bar{\Omega} = 1/2$) with Ar, N_2, and O_2 are shown for a variety of values of Δj for both spin–orbit conserving collisions, $\bar{\Omega}' = 1/2$, and spin–orbit changing collisions, $\bar{\Omega}' = 3/2$.[29] The integral steric asymmetry is defined such that a positive value corresponds to a preference for collisions at the N-end of the molecule, $\theta_E = 180°$: see Eq. (53).

Where available, theoretical results in the form of QM calculations and QCTs are included in the figure for comparison. Note that there are no QCT calculations for the spin–orbit changing manifold, as the QCT calculations treat NO(X) as a closed shell molecule. As noted above, the approximate QM data for NO(X) + N_2 were performed treating N_2 as a pseudo-atom.

As can be seen in Fig. 4, at low and middle $\Delta j = j' - j$, all three systems exhibit distinct oscillations in $S(z)$, with a tendency for more positive values for odd Δj and more negative values for even Δj transitions. In the region above about $\Delta j = 12$, the oscillations die out and the steric asymmetry increases in the positive direction. While the QM calculations reproduce well the position

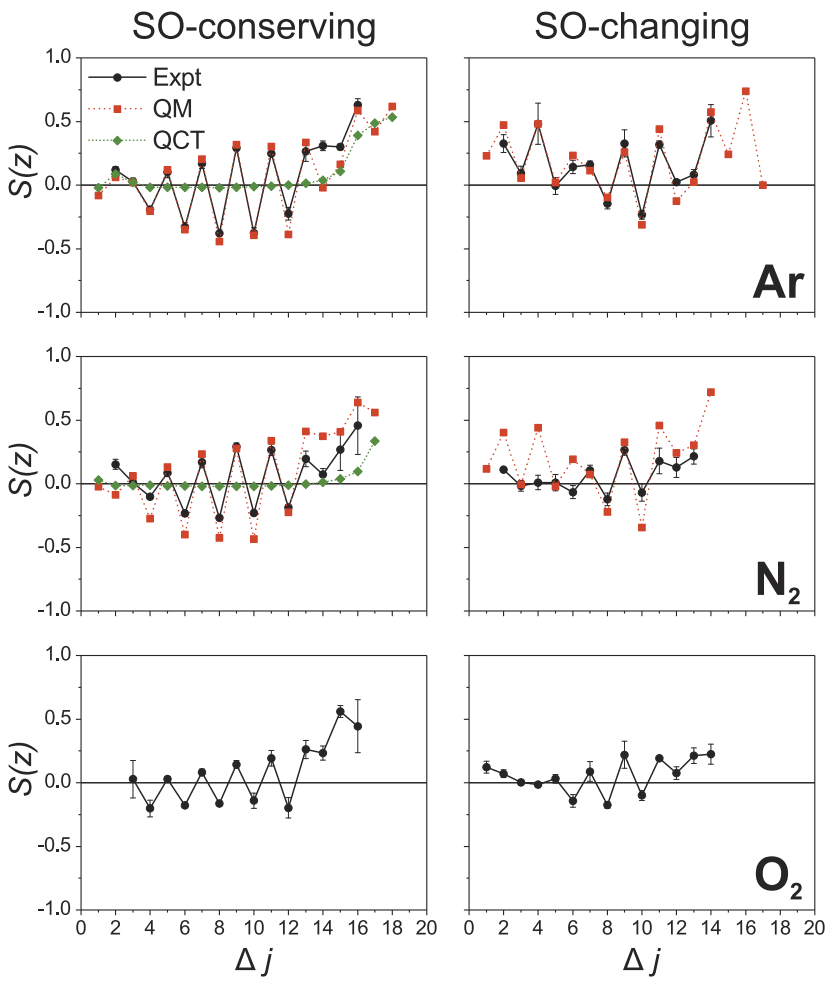

FIG. 4. Integral *z*-axis steric asymmetries, $S(z)$, as a function of Δj for collisions of NO($X^2\Pi$; $|j = 1/2$, $\bar{\Omega} = 1/2$, ***E***$\rangle$ with Ar (top), N_2 (middle), and O_2 (bottom), for spin–orbit conserving (left) and spin–orbit changing (right) transitions to the final *e* states. The plots for NO(X) + Ar and NO(X) + O_2 have been adapted from Ref. 29. The positive values of $S(z)$ correspond to preferential scattering off the N-end of NO. The experimental data are represented in black, the QM data are represented in red, and the QCT data are represented in green. The experiments were performed at the following collision energies: NO(X) + Ar (spin–orbit conserving transitions) 530 cm^{-1}; NO(X) + Ar (spin–orbit changing transitions) 651 cm^{-1}; NO(X) + N_2 845 cm^{-1}; and NO(X) + O_2 550 cm^{-1}.[29]

and magnitude of the oscillations observed experimentally at all Δj, the QCT calculations for collisions of NO(X) with Ar and N_2 predict almost no *z*-axis steric preference at low and middle Δj but agree with the experiment and the QM calculations in the high Δj region. These findings indicate the quantum nature of the inelastic scattering of NO in the region below $\Delta j \simeq 12$ and allow rationalization of the region above $\Delta j \simeq 12$ in terms of classical arguments.[23,37] In a QCT theoretical study on NO(X) + He, it has also been shown that at the N-end of the potential, the collision partner is able to penetrate further into the repulsive region, and thus, transitions involving higher rotational energy transfer (larger Δj) are more likely to occur at the N-end than at the O-end of the NO molecule.[38]

The oscillations in the low and middle Δj ranges can be quantitatively reproduced employing a quasi-quantum treatment (QQT),[39] which is based on a hard-shell NO potential. The model reveals that the alternating preference for N-end and O-end collisions is due to constructive and destructive interferences between trajectories at the two ends of the molecule.[29] Furthermore, due to the lack of attractive forces in the QQT model, the results imply that it is to a large extent the repulsive parts of the potential that are responsible for the observed oscillations.

Comparison between the data for the spin–orbit conserving and the spin–orbit changing data, in the left and right panels of Fig. 4 respectively, shows an overall increased preference for N-end collisions in the spin–orbit changing manifold; although the same oscillations as for the spin–orbit conserving manifold persist, the integral *z*-axis steric asymmetry is shifted toward positive values. The reason for this shift can be understood by considering the underlying PESs for the spin–orbit conserving and changing transitions. The NO(X) + Rg systems involve two PESs, one of A' and one of A'' symmetry. In Hund's case (a) description, which applies reasonably well to NO for the lowest and middle *j*-values, spin–orbit conserving transitions can be approximated to occur on the sum of the two potentials, while spin–orbit changing transitions can be approximated to occur on the difference potential.[40,41] The difference potential has a pronounced repulsive wall at the O-end but is purely attractive at the N-end so that, overall, collisions at the N-end are favored for spin–orbit changing transitions.[29]

The dynamics of collisions of NO(X) with N_2 and O_2 are, of course, more complicated than those of NO with a rare gas atom. The molecular collision partners can now also be rotationally excited, and so, the internal and translational energies of the detected NO may be correlated with different quantum states of the partner product. However, the main features in the integral steric asymmetry data appear to be similar for NO(X) + Ar and NO(X) + N_2/O_2, indicating that the measured (and calculated) quantities are signatures of the scattered NO species, which are only subtly modified by the nature of the collision partner. Perhaps, the biggest difference can be seen between the NO(X) + Ar and the NO(X) + O_2 data: the magnitudes of $S(z)$ are clearly smaller and exhibit less of a curved profile with increasing Δj for O_2 than for Ar. It has been speculated that these differences arise from a more isotropic and possibly more attractive potential for NO + O_2 but may also reflect the more complex electronic structure of the NO–O_2 system compared to collisions of NO with the closed shell collision partners.[29] An accurate theoretical description would clearly be desirable to gain further insights into the finer details of the scattering dynamics of the NO(X) + diatom systems.

C. OH($X^2\Pi$) + Ar integral and differential effects

A series of comprehensive experiments with the aim of investigating the integral steric effects in collisions of OH($X^2\Pi_{3/2}$) with Ar were carried out by ter Meulen *et al.* at a collision energy of E_{coll} = 746 cm^{-1} using laser induced fluorescence (LIF) as a state specific detection method.[26,42,43] In their experiments, the OH(X) $|j = 3/2, \bar{\Omega} = 3/2, f\rangle$ initial state was selected using two different hexapole arrangements: one consisted of a single hexapole and the other used a tandem of consecutive hexapoles. The two possible $\bar{m}_E$ states resulting from that selection, $\bar{m}_E$ = 1/2 and 3/2, are split in energy by the Stark effect upon application of a static electric field that orients the OH bond-axis.

The QM integral steric asymmetries, for the inelastic scattering of OH(X) with Ar, as a function of j', are shown in Fig. 5, for scattering from the two initial $|j = 3/2, \bar{\Omega} = 3/2, \bar{m}_E, \boldsymbol{E}\rangle$ states, where $\bar{m}_E$ = 1/2 and 3/2 in the left and right panels, respectively. The two upper panels depict the orientation along the z-axis (coincident with $\boldsymbol{k}$, the initial relative velocity), and the lower panels correspond to orientation along the x-axis (recall that $\boldsymbol{k} - \boldsymbol{k}'$ defines the xz-plane). Before entering into the discussion of these results, it is pertinent to examine the extent of agreement with the existing experimental data.

The comparison between the experimental results of van Beek *et al.*[26] for the z-axis polarization and those from QM calculations using the formalism detailed in Sec. II B is shown in the top and bottom panels of Fig. 6 for spin-conserving, $\bar{\Omega} = 3/2 \rightarrow \bar{\Omega}' = 3/2$, and spin–orbit changing collisions, $\bar{\Omega} = 3/2 \rightarrow \bar{\Omega}' = 1/2$, respectively. In this figure, the left and right panels correspond to collisions leading to e and f final Λ-doublet states, respectively. In addition, within each panel, the two sets of experimental data obtained with single and double hexapole selection are also shown, along with their respective theoretical simulations. The theoretical results for the OH($j = 3/2, \bar{\Omega} = 3/2$) initial state have been calculated by weighting the contribution of the $\bar{m}_E$ = 1/2 and 3/2 states shown in Fig. 5 according to the experimental conditions: 1:2.6 for the single hexapole and 1:15.8 for the double hexapole.[26,42] In the two cases, the values of the mixing parameters are different for the two $\bar{m}_E$ states. For $\bar{m}_E$ = 1/2, $|\alpha| = 0.66$ and $|\beta| = 1.25$, while for $\bar{m}_E$ = 3/2, $\alpha = 0.88$ and $\beta = 1.10$ at an electric field strength of E = 7.5 kV cm^{-1}. Note that in the original article by van Beek *et al.*,[26] the α and β coefficients are exchanged with respect to those used here, and in addition, their parameters are normalized to $\alpha^2 + \beta^2$

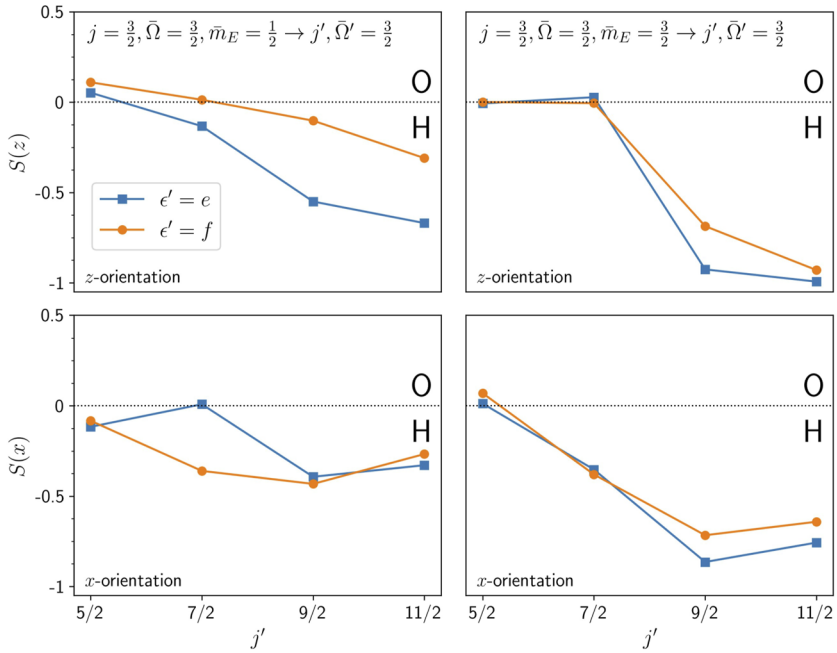

FIG. 5. Integral z-axis (top row) and x-axis (bottom row) steric asymmetries [$S(z/x)$] for inelastic scattering of OH(X) with Ar from the initial $|\bar{\Omega} = \frac{3}{2}, j = \frac{3}{2}\rangle$ state, at a collision energy of 746 cm^{-1}. The panels show QM calculations for spin–orbit conserving scattering from the initial $\bar{m}_E$ = 1/2 (left) and 3/2 (right) states. In both cases, transitions are shown for both final Λ-doublets with the f and e states shown with orange circles and blue squares, respectively. The negative $S(z)$ values ($\sigma^{+z} > \sigma^{-z}$) correspond to preferential scattering off the H-end of OH, and the negative $S(x)$ values ($\sigma^{-x} > \sigma^{+x}$) correspond to *repulsive* (i.e., near-side) scattering off the H-end of the OH molecule.

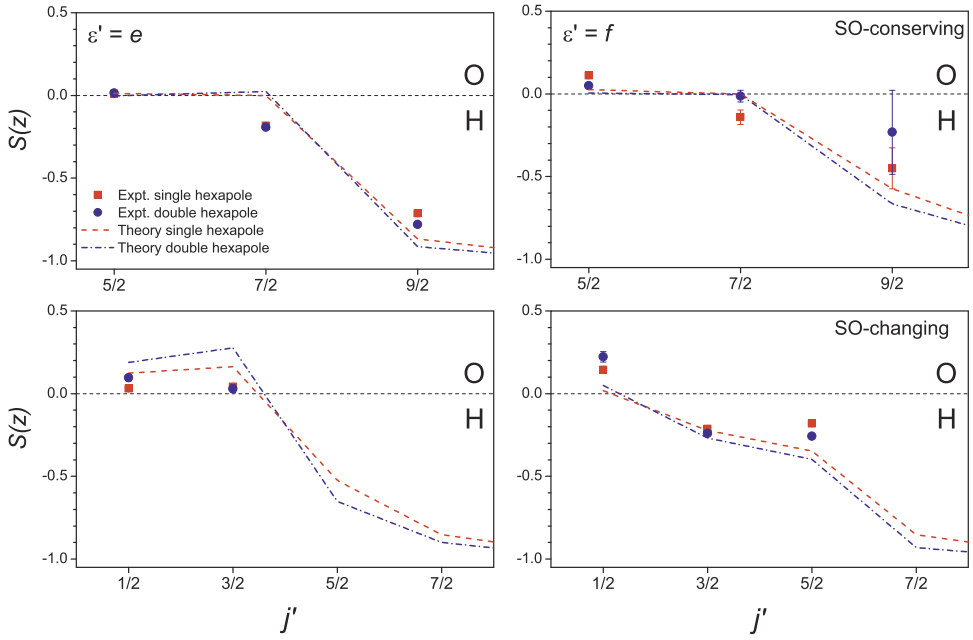

FIG. 6. Comparison of the QM calculations and the experimental integral steric asymmetry, $S(z)$, of van Beek *et al.*[26] for the final *e* (left) and *f* (right) Λ-doublets for OH(X) + Ar at a collision energy of 746 cm^{-1}. The upper panels show data for spin–orbit conserving transitions, while the lower panels show data for the spin–orbit changing transitions. Experimental data for the initial $|\bar{\Omega} = \frac{3}{2}, j = \frac{3}{2}\rangle$ state is shown by points, while theory is shown by dashed lines. The red and blue lines correspond to the passage of the OH(X) molecules through either a single or a double hexapole, respectively, before the collision. Note that negative $S(z)$ implies a preference for scattering off the H-end of the OH molecule.

= 1, whereas the sum of the squares used in this work is 2. With these parameters, the average orientations of $\langle\cos\Theta_{\mu E}\rangle_{1/2} = 0.162$ and $\langle\cos\Theta_{\mu E}\rangle_{3/2} = 0.574$ are achieved. As can be seen in Fig. 2, not only the average orientation but also the resulting distributions of internuclear axes are remarkably different for the two m_E states. The average orientation (including both $\bar{m}_E$ states) with the double hexapole ($\langle\cos\Theta_{\mu E}\rangle = 0.549$) was higher than with the single hexapole ($\langle\cos\Theta_{\mu E}\rangle = 0.458$) due to the larger proportion of molecules in the more highly oriented $\bar{m}_E = 3/2$ state.[26] For comparison, at the limit of an infinite field with the pure $\bar{m}_E$ state, the maximal orientation achievable is $\langle\cos\Theta_{\mu E}\rangle^{\infty}_{3/2} = 0.6$, and the resulting distribution of internuclear axes is also shown in Fig. 2 as the blue shaded area, which barely differs from the experimental one (pink shaded area).

For spin–orbit conserving collisions, the agreement between the experimental results and the QM calculations is fairly good for both final Λ-doublet states, and, as expected, the QM data presented here are practically identical to the QM results shown in Ref. 26 using the same PES (not shown here). In principle, it is expected that the absolute magnitude of ISAs should be larger for the double hexapole than for the single hexapole experiments due to the increase in orientation achieved in this experimental setup.[26] This is experimentally observed for the spin–orbit conserving, final *e* state; however, the trend appears to be reversed for larger transitions to the final *f* state. This is attributed to the small integral cross sections of these states along with the residual population of these states that pass through the hexapole.[26] van Beek *et al.* have also studied the steric effect in the spin–orbit changing collisions of $OH(j = 3/2, \tilde{\Omega} = 3/2) \rightarrow OH(\tilde{\Omega}' = 1/2)$,[26,43] whose comparison with the present QM results is shown in the bottom panels for final *f* and *e* states. The agreement with the present theoretical calculations is also fairly good, comparable to that obtained for $\tilde{\Omega}$ conserving collisions.

Let us return to Fig. 5, and consider first the *z*-axis polarized steric asymmetry for OH(X) + Ar for spin–orbit conserving transitions. For both values of $\bar{m}_E$, the value of $S(z)$ decreases with increasing rotational energy transfer, although its value is considerably less negative for $j' > 7/2$ with $\bar{m}_E = 1/2$, due to the lower degree of orientation as a consequence of the distribution of axes not being strictly along the *z*-axis (see Fig. 2). The results indicate a very slight preference for O-end collisions [positive $S(z)$] for low rotational energy transfer collisions, $j' \leq 7/2$, but a definitively stronger preference for H-end collisions [negative $S(z)$] at higher j' values. This may be explained via largely classical mechanisms. The potential at the H-end of the molecule extends much further from the center-of-mass than the O-end of the molecule; collisions occurring when Ar approaches the H-end of the molecule are able to penetrate further into the repulsive core of the potential, allowing for higher rotational energy transfer. Meanwhile, trajectories approaching the O-end of the molecule almost hit the center-of-mass of the molecule and therefore cannot lead to rotational energy transfer into high rotational states. The steric effect depends on the final Λ-doublet of the transition [unlike the collisions of NO(X) with Ar; see Refs. 23 and 25]. $S(z)$ takes more negative values for transitions into the final *e* state than for transitions into the final *f* state. This is observed more strongly for $\bar{m}_E = 1/2$ than for $\bar{m}_E = 3/2$ and also increases as a function of Δj. There is currently no simple explanation for this behavior.[44] The trend is also observed in the experimental data of van Beek *et al.*[26]

The magnitude of $S(z/x)$ is similar for the orientations along the *z*- and *x*-axes, and both also follow a roughly similar, monotonic trend with respect to Δj. The *x*-axis steric effect (lower panels of Fig. 5) also depends on the final Λ-doublet state of the transition, again somewhat more strongly for the $\bar{m}_E = 1/2$ state than for the $\bar{m}_E = 3/2$ state, with a larger difference observed for larger rotational energy transfer. The theoretical predictions indicate that $S(x)$

becomes negative (preference for H-end collisions) for $j' \geq 7/2$ values, but at the highest j', it levels off. The trend observed for the x-axis steric effect may be understood in a similar way to that of the z-axis, based upon differences in the PES of the OH(X) + Ar collision. Collisions corresponding to $+x/-x$ scattering are equivalent to repulsive "near-side" collisions at the O/H-ends of the molecule; as such, the preference for H-end collisions at high j' may be understood in terms of the larger extension of the potential as in the z-axis case. For low rotational energy transfer, where the attractive parts of the PES play a more important role in determining the scattering dynamics, the small values of $S(x)$ and $S(z)$ may be understood in terms of the balance between repulsive "near-side" scattering and attractive "far-side" scattering (see further below).

The QM DCSs (multiplied by $\sin\theta$) for the inelastic scattering of $OH(X^2\Pi_{3/2})$ + Ar for the $|j = 3/2,\ \tilde{m}_E = 3/2,\ \tilde{\Omega} = 3/2,\ E = \infty\rangle \rightarrow |\tilde{\Omega}' = 3/2, \varepsilon' = e\rangle$ transitions are shown in Fig. 7, for $j' = 5/2 - 11/2$ at a collision energy of 746 cm^{-1}. In each case, the DCSs for parallel and anti-parallel orientation of $\boldsymbol{r}$ along the x- and z-axes are shown, alongside that for orientation along the y-axis, which is equivalent in the $+y$ and $-y$ directions, as only alignment terms, not

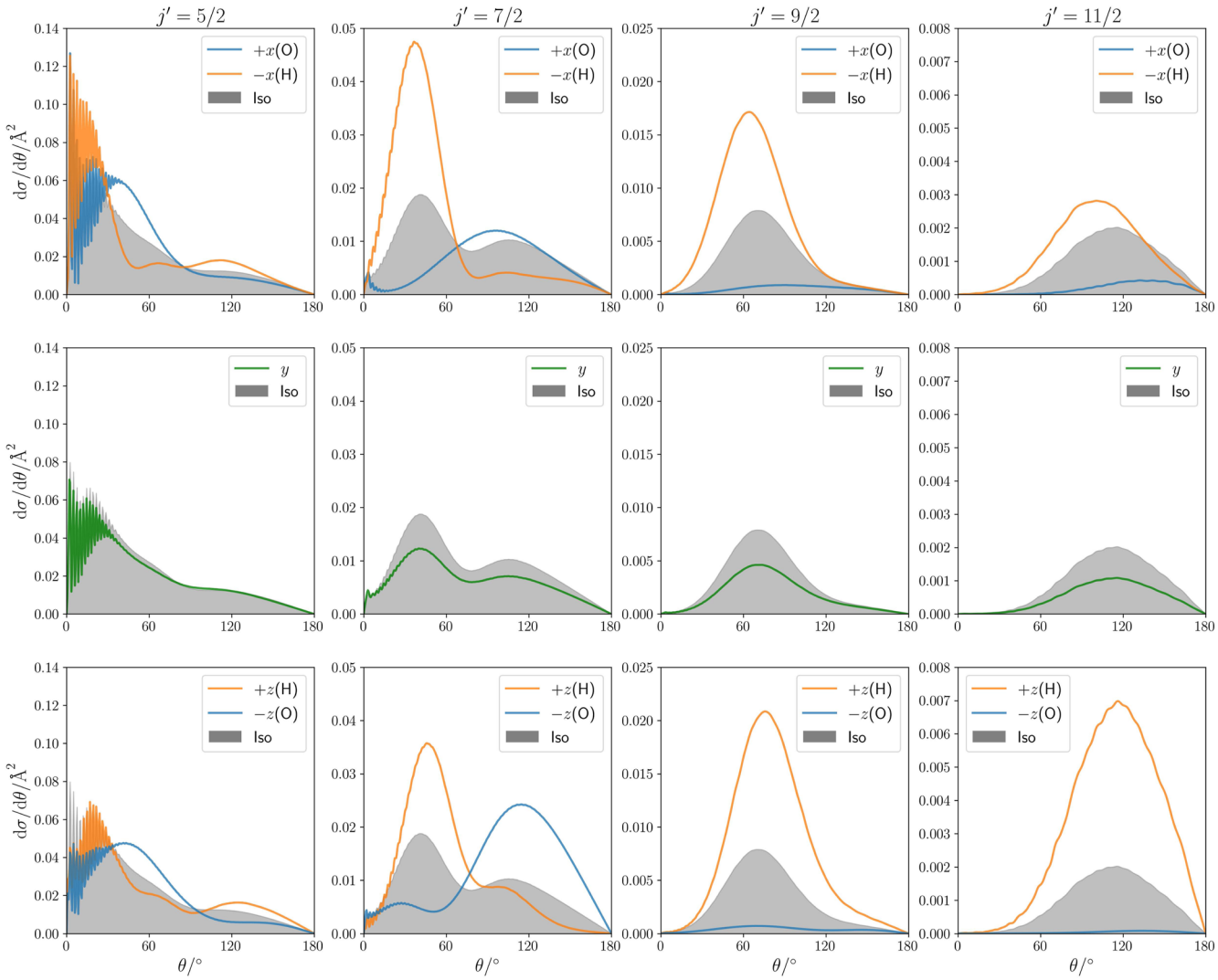

FIG. 7. Differential cross sections for the energetically accessible j', e final states of the OH(X) + Ar system at a collision energy of 746 cm^{-1}, in the high-field limit ($\alpha = \beta = 1$), starting from the $|\tilde{\Omega} = 3/2, j = 3/2, \tilde{m}_E = 3/2\rangle$ initial state. The top row for each panel is for orientation along the x-axis: $+x$(O) ($\theta_E = 90°$, $\phi_E = 0°$) and $-x$(H) ($\theta_E = 90°$, $\phi_E = 180°$) are shown in blue and orange, respectively. The middle row shows orientation along the y-axis, in which the $+y$ ($\theta_E = 90°$, $\phi_E = 90°$) and $-y$ ($\theta_E = 90°$, $\phi_E = 270°$) orientations are equivalent, as shown in green. The bottom row shows orientation along the z-axis: $+z$(H) and $-z$(O) data are shown in orange and blue, respectively. The isotropic DCS, proportional to $R_0^{(0)}(\theta)$, in each case is indicated by the gray shaded area. Note that for $j > 1/2$, the y polarization also contains alignment terms (k even, $q = 0$) and is no longer corresponding to $\tilde{R}_0^{(0)}(\theta)$.

orientation terms, contribute. In each panel, the DCS in an isotropic electric field, the average of the DCS for initial e and f states, is also shown. Note that in this figure, the reference to O and H on the $+x$(O) and $-x$(H) and $+z$(O) and $-z$(H) labels refers to the case of "near-side" repulsive scattering.

The general trends observed in the differential steric effect are essentially independent of the x- or z-choice of orientation axis. In both cases, collisions imparting substantial rotational energy transfer occur with the H-end of the molecule, leading to sideway scattering for intermediate j' and to backward scattering for the highest j'. Furthermore, fast diffraction oscillations alongside glory scattering at extreme forward scattering angles ($0^\circ \le \theta \le 20^\circ$) are also observed for both z and x polarizations. The z-axis oriented DCSs in Fig. 7, as in the case of the integral steric effect, show an increasing preference for H-end orientation as a function of increasing rotational state to the point that, for $j' = 11/2$, $d\sigma_O - d\sigma_H \approx -d\sigma_H$. This feature can be explained by resorting to the classical mechanisms discussed with respect to $S(z)$. As noted above, since the center of mass of the molecule almost lies on the O atom and the potential dies off very quickly around this atom, head-on collisions with the O-end of the OH molecule are largely ineffective in achieving rotational energy transfer, while collisions at the H-end of the molecule may produce a significant torque that causes the rotation of the molecule much more readily. As in the case of bond-oriented collisions of NO(X),[23,25] similar features are observed in the DCSs for both the z-axis orientations, however, the intensity of these peaks varies for the two orientations. Unlike the case of NO(X), the position of the peaks in the DCS is significantly shifted relative to one another for intermediate and high Δj.

While the x-axis oriented DCSs exhibit similar features to those of the z-axis polarization, since the same $R_0^{(0)}(\theta)$ term in Eq. (45) is at work, some differences are observed related to the $R_0^{(1)}(\theta)$ and $R_1^{(1)}(\theta)$ moments that account for the differential steric asymmetry effect when the OH bond is oriented along either the z- or x-axis, respectively. As in the integral steric effect, a preponderance of scattering with H-side orientation (with the electric field along $-x$) with respect to the O-side orientation (electric field along $+x$) is observed with increasing j', corresponding to an increasing preference for repulsive "near-side" collisions at the H-side of the molecule, where the extent of the repulsive potential is larger. The shift in peak position for the $\pm x$ orientations may be rationalized in a similar way to that discussed in terms of the z-axis, in which more "head-on" trajectories are required to achieve rotational energy transfer at the O-side of the molecule into the same state, leading to more backward scattering. Note that the difference between scattering from these two "side-on" orientations is not as large in comparison with scattering in the two "end-on" orientations (Fig. 5). This implies that the preference for scattering off the H- or O-end of the OH molecule is less strong when the atom approaches from the "flatter" side of the molecule.

As noted above, in the forward scattering region, for low Δj transitions, strong diffraction oscillations are observed for all the bond axis orientations shown in Fig. 7. Furthermore, for the transition to $j' = 5/2$, a strong preference for the $-x$ orientation is observed in the forward scattered region. This can be explained in terms of a preference for attractive, "far-side" scattering off the O-side of the molecule. However, the strong oscillations observed particularly in the x-axis orientation are likely to arise from interference between "far-side" and "near-side" collisions off the two ends of the molecule, suggesting that both types of collision play an important role in scattering in the forward direction for low Δj transitions.

IV. CONCLUSION

A general formalism has been presented to describe the stereodynamics of a $^2\Pi$ molecule oriented in an electric field and colliding with a rare gas or an unoriented molecule. Its utility and versatility have then been displayed through a set of specific examples, helping us provide insights into how the anisotropy of the PES produces different outcomes upon the sampling of different regions. This is a powerful tool to assist in the unraveling of steric effects in reaction dynamics.

The equations presented are applicable to other molecules with closely spaced energy levels of opposite parity, such as symmetric top and near-symmetric top molecules. However, in many cases, states above the ground state will also be oriented in the electric field, and so, the theory presented here would need to be developed further.

Moving forward to more complex systems, i.e., those with two polarized molecules, this formalism can be expanded further. In that case, it could be that both molecules have their initial angular momenta polarized,[45] or their initial bond axis distributions polarized, or a combination of the two. An extension to such systems would represent a step-change toward systems with more relevance to real world applications.

ACKNOWLEDGMENTS

F.J.A. acknowledges funding by the Spanish Ministry of Science and Innovation (Grant No. PID2021-122839NB-I00). P.G.J. acknowledges Grant Nos. PID2020-113147GA-I00 and PID2023-147215NB-I00 funded by MCIN/AEI/10.13039/501100011033 Spanish Ministry of Science and Innovation, and FEDER, UE. M.B. gratefully acknowledges the support provided by the UK Engineering and Physical Sciences Research Council (EPSRC) for funding through Program Grant No. EP/T021675/1. A CC-BY license is applied to the author accepted manuscript arising from this submission, in accordance with UKRI open access conditions.

AUTHOR DECLARATIONS

Conflict of Interest

The authors have no conflicts to disclose.

Author Contributions

M.M. and M.S. contributed equally to this work.

Max McCrea: Formal analysis (equal); Writing – original draft (equal). **Matt Strutton**: Formal analysis (equal); Writing – original draft (equal). **Josh Featherstone**: Methodology (equal); Software (equal); Supervision (equal). **Cornelia G. Heid**: Formal analysis (equal); Writing – review & editing (equal). **Mark Brouard**: Conceptualization (equal); Formal analysis (equal); Writing – review &

editing (equal). **Pablo G. Jambrina**: Conceptualization (equal); Formal analysis (equal); Writing – review & editing (equal). **F. Javier Aoiz**: Conceptualization (equal); Formal analysis (equal); Writing – original draft (equal); Writing – review & editing (equal).

DATA AVAILABILITY

The data that support the findings of this study are available from the corresponding author upon reasonable request.

APPENDIX A: MATRIX OF THE SCATTERING AMPLITUDE PRODUCTS

For given j, $\bar{\Omega}$, j', and $\bar{\Omega}'$, the products of scattering amplitudes, $Q_{m_1\varepsilon_1\ m_2\varepsilon_2}$, Eq. (30), can be considered as the matrix elements of $\boldsymbol{Q}^{\varepsilon_1\ \varepsilon_2}$. Taking into account the symmetry of the scattering amplitudes, Eq. (23), the elements exhibit the following properties:

- Symmetry:

$$Q_{m_1\varepsilon_1\ m_2\varepsilon_2} = \varepsilon_1\varepsilon_2(-1)^{m_1+m_2-1}Q_{-m_1\varepsilon_1\ -m_2\varepsilon_2}. \tag{A1}$$

- Complex conjugate:

$$Q^*_{m_1\varepsilon_1\ m_2\varepsilon_2} = Q_{m_2\varepsilon_2\ m_1\varepsilon_1}. \tag{A2}$$

  Therefore, the $\boldsymbol{Q}^{\varepsilon\varepsilon}$ matrix is Hermitian (self-adjoint), while $\boldsymbol{Q}^{ef}$ and $\boldsymbol{Q}^{fe}$ are adjoint to each other in the Hermitian sense.
- If $m_1 = m_2 = m$,

$$Q_{m\varepsilon_1\ m\varepsilon_2} = \varepsilon_1\varepsilon_2\ Q_{-m\varepsilon_1\ -m\varepsilon_2}. \tag{A3}$$

- If, in addition, $\varepsilon_1 = \varepsilon_2 = \varepsilon$,

$$Q_{m\varepsilon\ m\varepsilon} = Q_{-m\varepsilon\ -m\varepsilon} = Q^*_{m\varepsilon\ m\varepsilon} = \sum_{m'}|F_{m'\varepsilon'\ m\varepsilon}|^2 = \sum_{m'}|F_{m'\varepsilon'\ -m\varepsilon}|^2, \tag{A4}$$

  and these elements are real.
- If $m_1 = m = -m_2$,

$$Q_{m\varepsilon_1-m\varepsilon_2} = -\varepsilon_1\varepsilon_2\ Q_{-m\varepsilon_1\ m\varepsilon_2} = Q^*_{-m\varepsilon_2\ m\varepsilon_1}. \tag{A5}$$

  As a consequence,

$$Q_{m\varepsilon_1-m\varepsilon_2} + Q_{m\varepsilon_2-m\varepsilon_1} = Q_{-m\varepsilon_1\ m\varepsilon_2} + Q_{-m\varepsilon_2\ m\varepsilon_1}. \tag{A6}$$

- If, in addition to $m_2 = -m_1$, $\varepsilon_1 = \varepsilon_2$,

$$Q_{m\varepsilon-m\varepsilon} = -Q_{-m\varepsilon\ \ m\varepsilon} = -Q^*_{m\varepsilon-m\varepsilon}, \tag{A7}$$

  that is, the matrix element is purely imaginary.
- If $m_1 \neq m_2$ and they are contiguous ($|m_1 - m_2| = 1$),

$$Q_{m_1\varepsilon_1-m_2\varepsilon_2} = \varepsilon_1\varepsilon_2\ Q_{-m_1\varepsilon_1\ m_2\varepsilon_2} = \varepsilon_1\varepsilon_2 Q^*_{m_2\varepsilon_2-m_1\varepsilon_1}. \tag{A8}$$

  If, in addition, $\varepsilon_1 \neq \varepsilon_2$,

$$Q_{m_1\varepsilon_1\ m_2\varepsilon_2} + Q_{m_1\varepsilon_2\ m_2\varepsilon_1} = Q_{-m_1\varepsilon_1-m_2\varepsilon_2} + Q_{-m_1\varepsilon_2-m_2\varepsilon_1}. \tag{A9}$$

APPENDIX B: DERIVATION OF THE *r*-PDDCSs

Using the relation[11]

$$D^j_{m_1m_E}(\phi,\theta,0)\ D^{j*}_{m_2m_E}(\phi,\theta,0) = \sum_{k,q}\left(\frac{2k+1}{2j+1}\right)\langle jm_1, k-q|jm_2\rangle\langle jm_E, k0|jm_E\rangle C_{k-q}(\theta,\phi), \tag{B1}$$

Eq. (31) may be rewritten as

$$\mathrm{d}\sigma(jm_E\ \bar{\Omega}\hat{E}\to j'\ \bar{\Omega}'\varepsilon') = \frac{1}{2}\left[\alpha^2\ T^{m_E}_{ee} + \alpha\beta\ T^{m_E}_{ef} + \beta^2\ T^{m_E}_{ff}\right], \tag{B2}$$

where

$$\begin{aligned} T^{m_E}_{\varepsilon\varepsilon} &= \sum_{k,q}\left(\frac{2k+1}{2j+1}\right)\langle jm_E, k0|jm_E\rangle \\ &\quad\times\sum_{m_1,m_2} C_{k-q}(\theta_E,\phi_E)\langle jm_1, k-q|jm_2\rangle Q_{m_1\varepsilon\ m_2\varepsilon} \\ &= \sum_{k}\left(\frac{2k+1}{2j+1}\right)\langle jm_E, k0|jm_E\rangle \\ &\quad\times\sum_{q} C_{kq}(\theta_E,\phi_E)\sum_{m}\langle jm, kq|j(m+q)\rangle Q_{m\varepsilon\ (m+q)\varepsilon} \end{aligned} \tag{B3}$$

and

$$\begin{aligned} T^{m_E}_{\varepsilon_1\varepsilon_2} &= \sum_{k}\left(\frac{2k+1}{2j+1}\right)\langle jm_E, k0|jm_E\rangle\sum_{q} C_{kq}(\theta_E,\phi_E) \\ &\quad\times\sum_{m}\langle jm, kq|j(m+q)\rangle(Q_{m\varepsilon_1\ (m+q)\varepsilon_2} + Q_{m\varepsilon_2(m+q)\varepsilon_1}). \end{aligned} \tag{B4}$$

Hence, making use of Eq. (32), we can write the averaged DCS as

$$\begin{aligned} &\left[\mathrm{d}\sigma(j\tilde{m}_E\bar{\Omega}\hat{E}\to j'\bar{\Omega}'\varepsilon')\right]^{\phi_E}_{\theta_E} \\ &= \frac{1}{4}\left[\alpha^2\ (T^{(\tilde{m}_E)}_{ee} + T^{(-\tilde{m}_E)}_{ee}) - |\alpha\beta|\ (T^{(\tilde{m}_E)}_{ef} - T^{(-\tilde{m}_E)}_{ef})\right. \\ &\quad\left. + \beta^2(T^{\tilde{m}_E}_{ff} + T^{(-\tilde{m}_E)}_{ff})\right] = \frac{1}{4}\left[\alpha^2\ T^{(ee)} - |\alpha\beta|\ T^{(ef)} + \beta^2\ T^{(ff)}\right], \end{aligned} \tag{B5}$$

where

$$\begin{aligned} T^{(\varepsilon\varepsilon)} &= T^{(\tilde{m}_E)}_{\varepsilon\varepsilon} + T^{(-\tilde{m}_E)}_{\varepsilon\varepsilon} = 2\sum_{k}\left(\frac{2k+1}{2j+1}\right)\langle j\tilde{m}_E, k0|j\tilde{m}_E\rangle \\ &\quad\times\delta_{k,\mathrm{even}}\sum_{q} C_{kq}(\theta_E,\phi_E)\sum_{m}\langle jm, kq|j(m+q)\rangle Q_{m\varepsilon\ (m+q)\varepsilon} \end{aligned} \tag{B6}$$

and

$$\begin{aligned} T^{(ef)} &= T^{(\tilde{m}_E)}_{ef} - T^{(-\tilde{m}_E)}_{ef} = 2\sum_{k}\left(\frac{2k+1}{2j+1}\right)\langle j\tilde{m}_E, k0|j\tilde{m}_E\rangle \\ &\quad\times\delta_{k,\mathrm{odd}}\sum_{q} C_{kq}(\theta_E,\phi_E)\sum_{m}\langle jm, kq|j(m+q)\rangle \\ &\quad\times(Q_{mf\ (m+q)e} + Q_{me\ (m+q)f}). \end{aligned} \tag{B7}$$

The Kronecker deltas arise from the properties of the $\langle jm_E, k0|jm_E\rangle$ Clebsch–Gordan coefficient for $m_E = \pm\bar{m}_E$.

Returning to Eq. (33), we note that the extrinsic polarization moment must be included in the expansion. Hence, if we insert these moments from Eq. (20), we obtain, for even values of k,

$$\begin{aligned}
&\left[\mathrm{d}\sigma(j\bar{m}_E\bar{\Omega}\hat{E}\to j'\bar{\Omega}'\varepsilon')\right]^{\phi_E}_{\theta_E,\ \text{even } k}\\
&\quad=\frac{1}{4}\alpha^2T^{(ee)}+\frac{1}{4}\beta^2T^{(ff)}=\frac{1}{2}\sum_{k=\text{even}}\left(\frac{2k+1}{2j+1}\right)\frac{\mathscr{A}_0^{(\text{even }k)}}{\langle j\bar{\Omega},k0|j\bar{\Omega}\rangle}\\
&\quad\times\sum_q C_{kq}(\theta_E,\phi_E)\sum_m\langle jm,kq|j(m+q)\rangle\left(\alpha^2Q_{me(m+q)e}\right.\\
&\quad\left.+\beta^2Q_{mf(m+q)f}\right)=\frac{1}{2(2j+1)}\sum_{k=\text{even}}(2k+1)\frac{\mathscr{A}_0^{(\text{even }k)}}{\langle j\bar{\Omega},k0|j\bar{\Omega}\rangle}\\
&\quad\times\sum_q C_{kq}(\theta_E,\phi_E)\sum_m\langle jm,kq|j(m+q)\rangle\sum_{\varepsilon=e,f}\gamma_\varepsilon^2\quad Q_{m\varepsilon(m+q)\varepsilon}
\end{aligned}\tag{B8}$$

and, for odd values of k,

$$\begin{aligned}
&\left[\mathrm{d}\sigma(j\bar{m}_E\bar{\Omega}\hat{E}\to j'\bar{\Omega}'\varepsilon')\right]^{\phi_E}_{\theta_E,\text{odd }k}\\
&\quad=-\frac{1}{4}|\alpha\beta|T^{(ef)}=\frac{1}{2}\sum_{k=\text{odd}}\left(\frac{2k+1}{2j+1}\right)\frac{\mathscr{A}_0^{(\text{odd }k)}}{\langle j\bar{\Omega},k0|j\bar{\Omega}\rangle}\sum_q C_{kq}(\theta_E,\phi_E)\\
&\quad\times\sum_m\langle jm,kq|j(m+q)\rangle(Q_{mf(m+q)e}+Q_{me(m+q)f})\\
&\quad=\frac{1}{2(2j+1)}\sum_{k=\text{odd}}(2k+1)\frac{\mathscr{A}_0^{(k)}}{\langle j\bar{\Omega},k0|j\bar{\Omega}\rangle}\sum_q C_{kq}(\theta_E,\phi_E)\\
&\quad\times\sum_m\langle jm,kq|j(m+q)\rangle\sum_{\substack{\varepsilon_1=e,f\\ \varepsilon_1\neq\varepsilon_2}}Q_{m\varepsilon_1(m+q)\varepsilon_2}.
\end{aligned}\tag{B9}$$

By comparison with Eq. (33), we obtain the expressions for the ***r***-PDDCSs seen in Eqs. (34) and (35).

APPENDIX C: RELATIONSHIP BETWEEN *j*-PDDCSs AND *r*-PDDCSs

The expression of the unnormalized ***j***-PDDCS, $U_q^{(k)}(\theta)$, for closed-shell molecules in terms of the scattering amplitudes is[8]

$$U_q^{(k)}(\theta)=\frac{\sigma}{2\pi}S_q^{(k)}(\theta)=\frac{1}{2j+1}\sum_m\langle jm,kq\,|j(m+q)\rangle Q_{m\ (m+q)},\tag{C1}$$

where $S_q^{(k)}(\theta)$ are the normalized PDDCSs. In the case of open-shell molecules from an initial j, $\bar{\Omega}$, ε to a final state j', $\bar{\Omega}'$, ε',

$$\left[U_q^{(k)}(\theta)\right]_{\varepsilon\to\varepsilon'}=\frac{1}{2j+1}\sum_m\langle jm,kq\,|j\ (m+q)\rangle Q_{m\varepsilon\ (m+q)\varepsilon}.\tag{C2}$$

If the initial state is a superposition of e and f states as that created by the orienting field,

$$\begin{aligned}
&\left[\mathrm{d}\sigma(j\bar{m}_E\bar{\Omega}\hat{E}\to j'\bar{\Omega}'\varepsilon')\right]^{\phi_E}_{\theta_E,\ \text{even } k}\\
&\quad=\sum_{k=\text{even}}\sum_q(2k+1)\langle j\bar{m}_E,k0|j\bar{m}_E\rangle C_{kq}(\theta_E,\phi_E)U_q^{(\text{even }k)}(\theta),
\end{aligned}\tag{C3}$$

where

$$\begin{aligned}
U_q^{(\text{even }k)}(\theta)&=\frac{1}{2(2j+1)}\sum_m\langle jm,kq|j(m+q)\rangle\\
&\quad\times\left(\alpha^2Q_{me\ (m+q)e}+\beta^2Q_{mf\ (m+q)f}\right).
\end{aligned}\tag{C4}$$

The odd term is

$$\begin{aligned}
&\left[\mathrm{d}\sigma\ (j\bar{m}_E\bar{\Omega}\hat{E}\to j'\bar{\Omega}'\varepsilon')\right]^{\phi_E}_{\theta_E,\ \text{odd }k}\\
&\quad=-|\alpha\beta|\sum_{k=\text{odd}}\sum_q(2k+1)\langle j\bar{m}_E,k0|j\bar{m}_E\rangle\\
&\quad\times C_{kq}(\theta_E,\phi_E)\ U_q^{(\text{odd }k)}(\theta),
\end{aligned}\tag{C5}$$

where

$$\begin{aligned}
U_q^{(\text{odd }k)}(\theta)&=\frac{1}{2(2j+1)}\sum_m\langle jm,kq|j\ (m+q)\rangle\\
&\quad\times\left(Q_{me\ (m+q)f}+Q_{mf\ (m+q)e}\right).
\end{aligned}\tag{C6}$$

Comparing Eqs. (C3) and (C5) with (B8) and (B9), it becomes evident that the relationship between ***r***- and ***j***-PDDCSs is

$$\tilde{R}_q^{(k)}(\theta)=\frac{U_q^{(k)}(\theta)}{\langle j\bar{\Omega},k0|j\bar{\Omega}\rangle}.\tag{C7}$$

For a superposition of e and f states, the symmetry rule governing the ***j***-PDDCSs in the case of open shell molecules is

$$U_q^{(k)}(\theta)=\varepsilon_1\varepsilon_2(-1)^k[U_q^{(k)}(\theta)]^*=\varepsilon_1\varepsilon_2(-1)^{k+q}\ U_{-q}^{(k)}(\theta).\tag{C8}$$

Although the ***j***-PDDCSs can be real or imaginary, the ***r***-PDDCSs are necessarily real. This implies that when $\varepsilon_1=\varepsilon_2$, k must be even. Conversely, when $\varepsilon_1\neq\varepsilon_2$, k must be odd.

REFERENCES

[1] R. D. Levine and R. B. Bernstein, *Molecular Reaction Dynamics and Chemical Reactivity* (Oxford University Press, New York, 1987).
[2] *Tutorials in Molecular Reaction Dynamics*, edited by M. Brouard and C. Vallance (Royal Society of Chemistry, Cambridge, 2012).
[3] A. T. J. B. Eppink and D. H. Parker, Rev. Sci. Instrum. **68**, 3477 (1997).
[4] D. W. Chandler and P. L. Houston, J. Chem. Phys. **87**, 1445 (1987).
[5] J. D. Barnwell, J. G. Loeser, and D. R. Herschbach, J. Phys. Chem. **87**, 2781 (1983).
[6] T. R. Sharples, J. G. Leng, T. F. M. Luxford, K. G. McKendrick, P. G. Jambrina, F. J. Aoiz, D. W. Chandler, and M. L. Costen, Nat. Chem. **10**, 1148 (2018).
[7] M. P. de Miranda, F. J. Aoiz, L. Bañares, and V. Sáez Rábanos, J. Chem. Phys. **111**, 5368 (1999).
[8] J. Aldegunde, M. P. de Miranda, J. M. Haigh, B. K. Kendrick, V. Sáez-Rábanos, and F. J. Aoiz, J. Phys. Chem. A **109**, 6200 (2005).
[9] J. Aldegunde, P. G. Jambrina, V. Sáez-Rábanos, M. P. de Miranda, and F. J. Aoiz, Phys. Chem. Chem. Phys. **12**, 13626 (2010).
[10] C. G. Heid, V. Walpole, M. Brouard, P. G. Jambrina, and F. J. Aoiz, Nat. Chem. **11**, 662 (2019).
[11] R. N. Zare, *Angular Momentum: Understanding Spatial Aspects in Chemistry and Physics* (Wiley-Interscience, 1988).
[12] F. J. Aoiz, M. Brouard, S. D. S. Gordon, B. Nichols, S. Stolte, and V. Walpole, Phys. Chem. Chem. Phys. **17**, 30210 (2015).
[13] M. H. Alexander, Faraday Discuss. **113**, 437 (1999).
[14] M. Lemeshko and B. Friedrich, J. Chem. Phys. **129**, 024301 (2008).

[15]M. Lemeshko, P. G. Jambrina, M. P. de Miranda, and B. Friedrich, J. Chem. Phys. **132**, 161102 (2010).
[16]S. Marinakis, B. J. Howard, F. J. Aoiz, and J. Kłos, Chem. Phys. Lett. **512**, 161 (2011).
[17]M. Brouard, H. Chadwick, C. J. Eyles, B. Hornung, B. Nichols, F. J. Aoiz, P. G. Jambrina, and S. Stolte, J. Chem. Phys. **138**, 104310 (2013).
[18]M. Brouard, H. Chadwick, C. J. Eyles, B. Hornung, B. Nichols, F. J. Aoiz, P. G. Jambrina, S. Stolte, and M. P. de Miranda, J. Chem. Phys. **138**, 104309 (2013).
[19]M. Brouard, H. Chadwick, S. D. S. Gordon, B. Hornung, B. Nichols, J. Kłos, F. J. Aoiz, and S. Stolte, J. Chem. Phys. **141**, 164306 (2014).
[20]T. V. Tscherbul and J. Kłos, Phys. Rev. A **103**, 062810 (2021).
[21]Z. Pavlovic, T. V. Tscherbul, H. R. Sadeghpour, G. C. Groenenboom, and A. Dalgarno, J. Phys. Chem. A **113**, 14670–14680 (2009).
[22]T. V. Tscherbul and R. V. Krems, Phys. Rev. Lett. **115**, 023201 (2015).
[23]M. Brouard, H. Chadwick, S. D. S. Gordon, B. Hornung, B. Nichols, F. J. Aoiz, and S. Stolte, J. Chem. Phys. **144**, 224301 (2016).
[24]K. Blum, *Density Matrix Theory and Applications*, 3rd ed. (Springer Science & Business Media, Heidelberg; Dordrecht; London; New York, 2012), Vol. 64.
[25]B. Nichols, H. Chadwick, S. D. S. Gordon, C. J. Eyles, B. Hornung, M. Brouard, M. H. Alexander, F. J. Aoiz, A. Gijsbertsen, and S. Stolte, Chem. Sci. **6**, 2202 (2015).
[26]M. C. van Beek, J. J. ter Meulen, and M. H. Alexander, J. Chem. Phys. **113**, 637 (2000).
[27]M. C. van Beek and J. J. ter Meulen, J. Chem. Phys. **115**, 1843 (2001).
[28]M. P. de Miranda, F. J. Aoiz, V. Sáez-Rábanos, and M. Brouard, J. Chem. Phys. **121**, 9830 (2004).
[29]M. Brouard, S. D. S. Gordon, A. Hackett Boyle, C. G. Heid, B. Nichols, V. Walpole, F. J. Aoiz, and S. Stolte, J. Chem. Phys. **146**, 014302 (2017).
[30]M. H. Alexander and S. Stolte, J. Chem. Phys. **112**, 8017 (2000).
[31]HIBRIDON is a package of programs for the time-independent quantum treatment of inelastic collisions and photodissociation written by M. H. Alexander, D. E. Manolopoulos, H. Werner, B. Follmeg with contributions P. F. Vohralik, D. Lemoine, G. Corey, R. Gordon, B. Johnson, T. Orlikowski, A. Berning, A. D. Esposti, C. Rist, P. Dagdigian, B. Pouilly, G. van der Sanden, M. Yang, F. de Weerd, S. Gregurick, and J. Kłos.
[32]D. E. Manolopoulos, J. Chem. Phys. **85**, 6425 (1986).
[33]M. H. Alexander and D. E. Manolopoulos, J. Chem. Phys. **86**, 2044 (1987).
[34]M. H. Alexander, J. Chem. Phys. **111**, 7426 (1999).
[35]B. Wen, H. Meyer, and J. Kłos, J. Chem. Phys. **132**, 154305 (2010).
[36]J. Klos, G. Chalasinski, M. T. Berry, R. A. Kendall, R. Burcl, M. M. Szczesniak, and S. M. Cybulski, J. Chem. Phys. **112**, 4952 (2000).
[37]M. Brouard, H. Chadwick, S. D. S. Gordon, B. Hornung, B. Nichols, F. J. Aoiz, and S. Stolte, J. Phys. Chem. A **119**, 12404 (2015).
[38]F. J. Aoiz, J. E. Verdasco, M. Brouard, J. Kłos, S. Marinakis, and S. Stolte, J. Phys. Chem. A **113**, 14636 (2009).
[39]A. Gijsbertsen, H. Linnartz, C. A. Taatjes, and S. Stolte, J. Am. Chem. Soc. **128**, 8777 (2006).
[40]M. H. Alexander, J. Chem. Phys. **76**, 5974 (1982).
[41]M. H. Alexander, Chem. Phys. **92**, 337 (1985).
[42]M. C. van Beek, J. J. ter Meulen, and M. H. Alexander, J. Chem. Phys. **113**, 628 (2000).
[43]M. C. van Beek, "Orientation effects in non-reactive collisions of OH," Ph.D. thesis, Katholieke Universiteit Nijmegen, 2001.
[44]K. Schreel and J. J. ter Meulen, J. Phys. Chem. A **101**, 7639 (1997).
[45]P. G. Jambrina, J. F. E. Croft, N. Balakrishnan, H. Guo, and F. J. Aoiz, Faraday Discuss. **251**, 104 (2024).